2015

VALIDITY OF LANDMARK SELECTION GIVEN DIFFERENT 3D SCAN PROCESSING PARAMETERS: LANDMARK LOCATION ON 3D MODELS OF YACCHI CRANIA

Mary-Margaret Murphy
University of Montana - Missoula

VALIDITY OF LANDMARK SELECTION GIVEN DIFFERENT 3D SCAN PROCESSING PARAMETERS: LANDMARK LOCATION ON 3D MODELS OF YACCHI CRANIA.

By

MARY-MARGARET MURPHY

Bachelor of Arts, The University of Montana, Missoula, Missoula 2010

Thesis

presented in partial fulfillment of the requirements
for the degree of

Master of Arts
in Anthropology

The University of Montana
Missoula, MT

December 2015

Approved by:

Sandy Ross, Dean of The Graduate School
Graduate School

Dr. Anna M. Prentiss, Chair
Department of Anthropology

Dr. Randall R. Skelton
Department of Anthropology

Dr. Bret W. Tobalske
Department of Biological Sciences

Murphy, Mary-Margaret, M.A., Fall 2015 Anthropology

Validity of landmark selection given different 3D scan processing parameters: landmark location on 3D models of Yacchi crania.

Chairperson: Dr. Anna M. Prentiss

This project tests the validity of the use of models generated with 3-D technology for the purposes of advancing craniometric methods in anthropology. The literature describing this technology as it is being incorporated and applied is focused on the classification of crania within population structure and evolutionary development. 3-D modeling methods create data that are static over time - as long as the collection and processing has a statistically insignificant impact on deviation from the original "true" sample.
This thesis is interested in the questions of data collection given variations between processing and metadata of 3-D models and uses data from crania recovered from cave burials discovered on Kume Island, Okinawa Japan. The collection has been captured in surface scans and by 3-D coordinate digitizer at different times by different researchers. Adapting 3-D scanning and 3-D medical imaging technology into anthropology is highly advantageous in terms of the quality and quantity of data that can be collected and shared. Models generated from surface imaging are an excellent tool for research that serves to transmit the information encoded in the skull. Recent surface imaging technology is very user friendly from a novice perspective. However, there are different capture and processing specifications between equipment and software, which have the potential to create error due to variation caused by the data capture processes. A review of recent research working to capitalize on 3-D models belies the variation in standards of imaging and model processing. These projects tend to be preferential to data that are collected from samples with a low error rate. Error could be due to deviation of symmetry or damage. However, recovered human crania in historic and archaeological contexts are unlikely to have low rates of damage.
In spite of the potential variations introduced by the applications of process parameters, there was no convincing degree of non-correspondence in correlation tests to two comparison approaches.
The ultimate goal is to develop guidelines for data collection and processing that are capable of capitalizing 3-D data from any of the available technologies and processing output that is computationally efficient as well as statistically correspondent.

Acknowledgments

A great measure of gratitude is due my thesis committee. Their patience and encouragement has made it possible for me to see this thesis through. After facing many practical and personal challenges, their guidance has served to keep me moving in a forward direction. Dr. Anna Prentiss accepted the challenge of steering my thesis work and committee, giving me the grounding and support I needed. Dr. Randall Skelton gave me some of the most incisive editing suggestions and thoughtful considerations for the development of the thesis study. Dr. Bret Tobalske has generously made time to join this committee and consider the research which is both inclusive and exclusive of his own body of study.

Deserving of my ongoing gratitude is Professor Noriko Seguchi, my first graduate advisor, without whom, I would have not had access to the sample data from which my research is based. With her continued support, access to materials, and returns to the University of Montana - this thesis was not only made possible, but has opened many new avenues of future research. Professor Tom Foor has been an advisor and excellent supporter since I first developed a fixation on anthropological statistics under his teachings. I am thankful for all his consultations and that he has always made time for my questions.

As a researcher, I must also thank those whose work and willingness to discuss and share with me have been key to rounding out my understanding of important concepts and research avenues beyond the realm of Anthropology. Dr. Shriram Hegde reached out around the world to offer suggested sources to explain complex concepts of matrix math and 3D rendering for this audience. Dr. Piotr Szymor made publications available from far outside the field which none the less resounded as they are trying to solve many of the same questions of technology integration for living subjects.

My family has stood by me during this long process and perfected baffled smiles while I often wax poetic about three dimensional visualization technology, the number of times I crashed the software so integral to my work, and brag about an inscrutable spreadsheet of raw data output. I am aware it has not been easy to bear witness to the struggles and I am grateful for the buoyancy that they always found for me when I thought I might be overwhelmed by the pursuit of this graduate degree.

Table of Contents

List of Figures

List of Tables

List of Equations

Chapter One

Chapter Outlines

This research sets out to address methodology issues regarding the correlative quality of direct captured Microscribe® (Revware, Raleigh, NC, USA) digitized craniometric data with that of data derived from processed digital ***mesh models***[1] of crania. Specifically, this thesis will test the validity of landmark points collected from models processed under two parameters against landmark point data collected from the original cranial materials using a standard for direct digital landmark point collection; the Microscribe® (Revware, Raleigh, NC, USA). The chapters in this thesis will explore the potential differences in methods and processing and the validity with which they can be expected to perform with the type of sample selected for this project.

In theory, the differences in landmark points selected among 3-D models processed with different resolution should have statistically negligible differences among them and from landmark points collected using a 3-D digitizer. If this proves to be accurate, it would support the use of a data conservative processing method for 3-D mesh models, meaning one that results in a smaller file size for improved utility for users and computers. The rational for a smaller, more conservative file size comes down to the processing power, graphics hardware, and software

[1] Terms in bold italics are included in Appendix 6: Definition of Terms, for clarification and definitions that apply to the context of this thesis.

rendering that working with 3-D graphics requires. This must be considered concurrently with the importance of maintaining congruence with the original physical materials. Statistically significant differences that might occur between the landmark points for processing and selection methods based on 3-D models of various sizes and resolutions would indicate the need for further research into methodological processes for the future application of 3-D scan data. This is especially important in terms of the kind of archaeological sample presented in this project which has by its nature a small sample size.

The *first chapter (Introduction)* will continue after the chapter outlines to discuss the motivation for this thesis in consideration of osteometric methodology and 3-D technology.

The *second chapter (Background)* will characterize the type of sample, and the technology applications to be reviewed and summarize of the recent and current research applications of 3-D data capture technology. Within the scope of the second chapter the utility of virtual models and methods of collecting the data represented by a 3-D digital model is discussed in the context of explicit experimental design and standards of collection and processing to maximize the interchangeability of data from the different three dimensional methods in use. Further, the theoretical background of validity testing is outlined to provide the framework in which the statistical models of testing are applied.

The treatments applied to the preparation of the 3-D coordinate data and 3-D models from their raw state to the fully processed models are described in the *third chapter (Materials and methods)*. Methods as applied to this test of the

validity of landmark data collected from historic human remains will assume that there is no statistically significant difference, between the landmark locations and ILD measured for each individual in the sample for all levels; direct digitizer, and four models representing the combinations of the processing parameters selected to represent variable mesh process states based on previous research. To test if the landmark locations should all yield the same - or convergent- result as the hypothesis, the sample will be compared for differences between the direct digitizer sample landmarks and the data collected from the 3-D digital models at the different processing levels.

The *fourth chapter (Results)* will provide the output of the statistical analysis undertaken in the third chapter and investigate the impact that the different levels of processing have on the landmark locations. Individual observers will typically have a consistent bias in choices made to determine the location of a landmark. Further, chosen locations for landmarks collected from the models could vary in spatial location or observation between different process parameter combinations as a result of the processes applied to the model. The scans are influenced by technological considerations and interactions between the scanner and target surface. The above described interpretive considerations must be included in the total interpretations of the results.

I will use the *fifth chapter (Discussions)* to clarify the implications that processing method variability has on the utility of 3-D crania models for osteometric research. The utility refers to the usefulness in terms of the interoperability of 3-D data; scan data and medical imaging, with direct data as collected using the

traditional craniometric measurements and three dimensional landmarks. Ideally, as proposed by the hypothesis of convergence, there is no convincing degree of statistical difference between landmarks collected either directly or from a 3-D model invariant of the processing methods as applied in this project.

The closing chapter of this thesis will return to the practice of 3-D data collection and the practical issues of application of 3-D models in research under evolutionary and development theoretical models as outlined in the introduction and literature review and discuss the state of current and future research and transmission of indirect data from human bones remains. This *sixth chapter (Conclusions)* will consider the methods as applied in the third, fourth, and fifth chapters and the types of craniometric data represented by the sample and models. This will be the opportunity for considerations about methodology for applied 3-D research. These considerations will review aspects of data collection best practices, baselines, and ***meta-data*** reporting that the results of this analysis would indicate as most appropriate for application to further extend this research.

Introduction

Anthropometric research is the study of measurements in human biology. Throughout the history of anthropology, a constant thread has been the desire to define or refute demarcation in the variation of the human form. The osteometric branch of anthropometrics studies the bone structures of the human body. The human cranium is a complex bone structure of the body and the result of formation and function - designed to house the large brain, organs of four specialized senses, and the functions of mastication and breathing (White and Folkens 2000). The

cranial structures develop in response to a genetic template influenced by environmental, mechanical, and hormonal factors during the development and adult life of a human. The forms of cranial structures are of particular interest to anthropology and medical sciences, which makes the ability to capture and identify details of the human crania one of particular importance (Slice et al. 2005; Ross et al. 2010; Williams and Slice 2010).

Tests of 3-D technology for the purposes of advancing osteometric understanding in anthropology are focused on the classification of crania within population structure and evolution (Ross and Williams 2008; Ross et al. 2010; Williams and Slice 2010; Saso et al. 2011; Jantz et al. 2013; Pinto et al. 2013; Abdel Fatah et al. 2014; Hale et al. 2014). Data collection and hypothesis testing is done with a particular research question in mind. This project is more interested in the sensitivity of data collection methods with regards to ***landmarks***, preservation and different capture technologies. As with the statistics that are applied to craniometric and geometric morphometrics, there is an assumption that the tools are appropriate and capable of collecting the necessary information to answer the research questions that are applied (Cignoni and Scopigno 2008).

This project is interested in data correspondence of landmarks collection using multiple 3-D representations of a historic sample that differ in processing parameters. Computational differences between technologies and differences in processing could create variations within synonymous samples. That alone would be a concern for a sample in perfect condition (Cignoni and Scopigno 2008). Cranial samples are rarely in perfect condition. In many cases, especially as research

considers further back in the human timeline, that the greater the significance of a sample to our knowledge about the represented population is inversely correlated with the completeness and preservation of that sample (Saso et al. 2011; Shearer et al. 2012).

Sample preservation is a contributor to uncontrolled error found within the sample. Crania can experience taphonomic damage at the time of recovery ranging from slight - such as deformation of symmetry that might be due to burial position, to severe - resulting from post-mortem ritual or unstable burial conditions. After recovery, preparation and curation are critical to maintain the integrity of bone remains, but even the most well-intentioned practices can fail, resulting in compromised preservation. Incomplete preservation is a problem when research methods do not consider and account for damage. But given the inconsistent nature of the preservation of human remains, incomplete does not devalue the importance of materials that constitute the best available representative sample of a population (Saso et al. 2011; Shearer et al. 2012).

Validity analysis is useful to assess whether the variability between the different processing methods is introducing systematic error, resulting in significantly different metric data. Application of Microscribe® (Revware, Raleigh, NC, USA) Digitizer landmarks is applied as the "gold-standard" metric against the collected sample coordinates is a criterion validity experiment that serves to evaluate the agreement between the samples under the differing processing conditions with the criterion method (Carmines and Zeller 1979).

Scanned data, technology and processing resolution and history within Medical Sciences and Biological Anthropology

Scanned data (Surface scan, CT, MRI) encompasses a broad range of digital capture and processing techniques that import real objects into a 3-D virtual environment. Theoretically, scanning technologies are capable of a very high degree of image resolution. However, all scanning methods still have limitations owing to the potential for variation and error at the various stages of capture, alignment, and reconstruction. Capture error in terms of 3-D scanning has to do with any interaction during the scanning process that interferes with accurate reproduction of the surface. Movement can cause error in all forms of surface scanning. Medical Imaging formats are sensitive to high density materials and metallic elements. Alignment and reconstruction are capable of moderating the degree of error found in a scan based model, however that moderation can be either positive or negative depending on the execution of the scan collection and the processes applied to the raw data to output mesh models.

Medical imaging has available many modes of data collection. Computed Tomography (CT) is used with a high frequency for both direct patient data collection as well as for the collection of research samples. This owes to the balance of factors of cost, availability, and the available variation of the technology that are available to medical researchers. The slices of a CT scan to be converted into a 3-D representation of a model, processed by separating the areas by the *voxel density*- which refers to the light or dark pixels produced on a sensor surface (x-ray film is an example of a sensor surface) converted to three-dimension by including the

depth of the slice. The amounts of radioactive particles that pass through a given sample are reflected on the resulting image as light areas for fewer transmitted particles to darker areas for more transmitted particles. Bone tends to appear lighter than soft tissue due to a greater density which prevents most of the particles from reaching the detector. Observers must rely on training and experience to determine the settings that are most appropriate as to the sample. Slice thickness, voxel density, and the radiographic tool are variable. Slices used could range from less than one to several mm thick. Features whose details fall between thicker slices will be difficult to interpret clearly and can carry high rates of error (Kim et al. 2012; Hale et al. 2014).

Laser and white-light 3-D surface scanning are non-invasive and non-radiologic methods of capturing an object in three-dimensions. Time-of-Flight laser triangulation and fringe projection pattern are the primary capture methods used to recreate a 3-D model of a real object. During a 3-D surface scan, the object causes an interference with the laser light or fringe pattern projected from a primary origin. The interference is observed by the optical sensors of the scanner which are offset from the projection origin and the interference is interpreted into a set of 3-D coordinates. The density of coordinates captured is dependent upon the instrument and the settings selected by the observer.

A laser 3-D surface scanner with an array of fine-tuned linear laser projections will capture a surface with a greater degree of detail than a single narrow-beam linear projection, which would have greater sensitivity than a wide-

beam laser projection. The array also capitalizes on multiple projection angles, which offer a larger geometric sample from which to calculate triangulated distance.

Fringe pattern, or white-light 3-D surface scans vary in color, pattern, and complexity. A single stationary surface capture involves the projection of one or more fringe patterns over a surface to calculate the surface shape by analysis of the deformation of the projected pattern. Increasing the number of patterns projected per stationary position increases the sample used to calculate the surface model. Multiple offset optical sensors are also a common feature of white-light systems. Multiple optical sensors at offset angles from the projection origin increase the density of capture of complex surfaces by observing the projection from different angles determined by the offset.

Holes, cavities, and curvature can interfere with surface scans due to the nature of projection and observation methods that are used to determine the surface. A cavity, such as the eye orbits will typically exhibit internal reflection that distorts the laser or pattern projection. The geometric properties of a void result in a difficulty for the optic sensor when determining the dimensions and boundaries of these forms. Voids are characterized by edges and undercut dimensions that confound surfaces scanners. Some problems can be overcome with careful capture and post processing. However, some problems in capture of surface variations are simply limitations of the technology. Multiple projections, and acute sensor offset can improve the sensitivity with which borders and edges of a void are calculated, but do not tend to improve the problems with internal reflection of a cavity.

Objects often cause problems with the accurate interpretation of their surface resulting from problems with the manner of interaction between the surface characteristics. Surface scanners have problems with high reflecting, and transmitting surfaces (translucent or dark, in both instances, allowing light to pass through rather than be reflected back). Dental enamel is a good example of a surface that is difficult to capture with benchmark resolution. The characteristics of reflection and transmission (translucence) found in dental enamel cause the optic sensor to see defects and holes in the surface that do not exist on the real object.

Benefits of this project

The benefits and importance of this project is driven by the growth and innovations in current biometric research. Many researchers have recently published methods in which qualitative osteological features are treated in a quantitative statistical methodology using digital surface data (Williams and Slice 2010; Sholts et al. 2011a; Garvin and Ruff 2012; Jantz et al. 2013; Pinto et al. 2013; Abdel Fatah et al. 2014). What many of these studies overlook is the importance of *standards of practice*. Creating a new pseudo-landmark or outline of a structure of interest (Athreya 2006; Thayer and Dobson 2010; Williams and Slice 2010; Saso et al. 2011; Fukase et al. 2012; Garvin and Ruff 2012; Shearer et al. 2012) is not unprecedented, but is arbitrary and risks increasing observer bias (and inter-observer error). Also, references for landmark definitions vary in documented research. Several important structural landmarks are the subject of debate as to their definition and real location. Prosthion location varies in definition and in the interpretation of definition between William W. Howells 1973 publication and that of Paul Martin from 1928 (White and Folkens 2000). The exact definitions and

utilizations of dacryon and maxillofrontale are often not clear or well rationalized when defining the interior of the eye orbit (Howells 1973). The research referenced above has been undertaken primarily to answer specific research questions about the sample population or biological theory, and therefore represents a challenge for generalization across populations and samples.

Biological characteristics such as species, age, and sex are categorical in nature, but for measurement and classification are difficult due to variation on a continuum. Scoring systems make use of identifiable traits generalized to a system. Making use of 3-D models for adapting a qualitative system to a quantitative measurement less bound by the subjective perspective of the observer is a strong argument for the use of the available scanning technologies.

Development and testing of *robust statistical methods* as defined by Huber (1981) to apply to analysis of 3-D surface data are under way (Mahfouz et al. 2007; Jantz et al. 2013; Abdel Fatah et al. 2014). In the future, these methods could be as well accepted as the two dimensional metric statistics traditionally applied to 2D data. For now, an imposing challenge is the consideration of the source and the consistency with which 3-D surface data is collected, processed, and applied. To ignore consistency creates problems for reproducing results, an integral part of the scientific method necessary to expand qualitative-to-quantitative morphometric theories from the initial test samples (typically either forensic or academic collections) to the medico-legal fields and historical and archaeological samples where data are rarely complete and often suffers small sample size and high variability (no clear correlation or high proportion of outliers). A forensic or

academic collection - hand-picked for use in the types of studies referred to above - typically rejects individuals from the sample for having some kind of preservation defect. But a sample drawn from a burial context or contemporary forensic context would have a strong chance of suffering defects that could compromise application of certain methods.

Chapter Two

Background

Digital data collection creates a data sample that is static over time. As long as collection and processing of the sample has a statistically insignificant impact on deviation from the original "true" sample, these data are very valuable to the advancement of the study of the human cranium. At the current time, it is possible to choose from several methods to capture information from a skull. Depending on the selected technology, scanning methods theoretically permit the most complete capture of cranial data currently possible; shape, scale, variations in coloration, physical texture of the surface, bone density, even the ability to reproduce physical models of scanned crania without the risks associated with casting.

The development of models for analysis is preferential to data that are collected from samples with a low error rate. Error could be due to deviation of symmetry or damage, however recovery of human crania in historic and archaeological contexts are more likely to have high rates of damage.

Two primary research tracks are invested in this type of cranial study; anthropology for biological and forensic purposes (Muramatsu et al. 2008; Ross and Williams 2008; Ross et al. 2010; Jantz et al. 2013; Hale et al. 2014), and medicine for the purposes of pathology and surgical study (Olszewski et al. 2006; Olszewski et al. 2007; Olszewski et al. 2010; Olszewski et al. 2013; Hale et al. 2014). While the outcome of interest is significantly different, the technologies and need for accuracy are similar. Medical research is more often able to make use of radiological medical imaging, such as CT and X-ray. However this is not always the

case, as there are times when soft tissue morphology is the subject of study (Wong et al. 2008).

Anthropology has traditionally applied straightforward tools for measurement that can be just as ready and reliable in the field as in the lab and relied heavily on the experience and training of the observer to qualify samples (Bass 2005; Hale et al. 2014). Developments in the field of anthropology in the previous decades have introduced new methods adapting technology that have become institutional. These methods include 3-D landmark point data collection as the first and now most common multidimensional method, up to surface and medical imaging scanning. The sensitivity of advanced technological methods arguably makes up for the increased data complexity in the light of the better, cheaper, faster, and readily available computational power to handle them. However, that is assuming that advanced methods in practice offer significant improvements in accuracy commensurate to stated benchmarks.

In recent years technology with the capacity to sense, collect, and process large scale data and render three-dimensional information has expanded. The push has been fueled as greater processing and computational powers have become more ubiquitous and less expensive in modern computers. The result is greater research access to advanced data collection technologies with the potential to change the ways researchers collect and interact with samples (Smith and Strait 2008).

To assume that advanced data collection technologies offer an improvement over their predecessors assumes that advanced methods collect data at a high

degree of resolution and accuracy (Smith and Strait 2008). The Z-Corp 3-D scanner used to collect the sample in this study has a benchmark capture resolution of 50 microns (= 0.05 millimeters), which should be more than sufficient to capture all but the finest foramina and surface irregularities expected to be found on the surface of a dry skull. This is not the case in practice. The human cranium is a complex object with surface characteristics that confound the optical sensors of surface scanners. In practice, the quality and accuracy of the surface that can be captured by 3-D surface scanners will be reduced. Weinberg and Kolar (2005) highlight the differences between the engineering and materials sciences applied to the testing and design of tools such as digitizers and 3-D scanners. When these tools are adopted by medical and anthropological sciences, with biological subjects and samples, the differences become a potential source of error, misuse, and misinterpretation. The set of facts outlined is a significant, but not an insurmountable consideration for biological sciences.

The report produced by Jantz et al. (2013) is a test of the biological classification power of 3-D data. The researchers implemented a systematic study of crania from a large, controlled forensic sample. The sample profile was made up entirely of known ethnicity and sex from modern North American individuals. The study set out to improve upon established and experimental methods of establishing the sex of an individual from characteristics of the cranium. Study samples were captured using CT scans and converted into 3-D models to continue the analysis in a digital environment. As part of the systematic experimental design, the authors tested multiple comparative mesh resolutions to determine the balance between precise models and computational efficiency. It is important to

point out that this study was designed with a controlled sample that rejected samples with evidence of pathology, peri- and post mortem damage or defects. Since the sample studied in Jantz et al. (2013) was controlled for many types of random variation, such that are common to a historical or archaeological sample, the application of their findings became important for this analysis.

Established qualitative methods for the determination of the sex for a set of human remains have a heavy reliance on post-cranial elements, training, and experience with the target populations. The authors of Jantz et al. (2013) focused on the cranium under the justification that forensic identification has to do with identifiable features and the cranium is not only the most complex bony region of the body, it is also the most individualized. The relative success of non-metric techniques is at least some degree attributable to the simple fact the skull reminds us of the human face which is a structure that a significant portion of our brain is dedicated to recognizing and differentiating.

Another significant contribution of the Jantz et al. (2013) paper is the introduction of a systematic study of "global analysis" of 3-D representations of cranial dimensions. It is not the first attempt at 3-D characterization and comparison of cranial features, but follows examples such as Saso et al. (2011), and Pinto et al. (2013). The authors developed a sample ***atlas***, which involved the creation of a model based the averages of the dimensions of the cranial sample.

Jantz et al. (2013) studied modern crania from a forensic collection using CT scans for capture and outlining a novel method of model reconstruction, alignment, statistical atlas creation for cranial analysis, and further developing a landmarking

method used by Hsiao et al. (1996; 2010) which used lateral cranial x-rays of subjects. The application of this process was to compare 'global' models (the 3-D reconstruction from CT scans of individual crania in contrast to their further study of linear inter-landmark distances) to each other and to the statistical atlas to look for areas of sex-specific variation. This identified areas of greater of lesser variation in relationship with the full cranial structure. When compared, they found that the areas of highest 'global' variation correlated to the highest ILD variation (PCA). In this project, the authors were able to further develop on the success of Hsiao et al. (1996; 2010) in seriating a sample of crania along known sex by using cranial variation from a CT scan data set instead of lateral cranial x-ray images.

Using a segmented region of interest – the central nasal-frontal area of the cranium, Saso et al. (2011) experimented with comparison between topographic segments of samples and a reference model. The reference model was a selected specimen from the sample, so no modifications were made. This contrasts the atlas method employed by Jantz et al. (2013). The segmentation was developed to characterize the supra-orbital structures medially and laterally and applied to questions regarding population structure the authors hoped could be inferred from the development of the frontal bone. The study undertaken is of particular interest to this project because the authors included samples in the data set that were incomplete and suffered varied degrees of taphonomic damage. The experimental design was explicit in describing the scanning details, such as the average number of ***faces***, the segmentation steps applied, and the use of an individual from the sample as the base model for comparison. The method of segmentation utilized a topographic effect based on the calculated heights of the points, perpendicular to a

reference grid generated during the segmentation process. The models were rendered from capture scans set to a very high resolution, which may have been greater than necessary. This may have been one of the reasons the authors chose to use a segmentation method to simplify the area of study. However, it is significant that the authors reported this type of meta-data and did so in terminology rational to the type of 3-D mesh that was captured and studied. The segmentation and application of the topographical system becomes a data reduction from the whole cranium to the region of interest, then from 3-D dimensional surface data to two-dimensional points and outlines which were more conducive with the applied statistical tests.

Pinto et al. (2013) is a unique study of the classification power of multi-dimensional structures. The paper presents the authors attempt to solve the difficult problems of ***homology*** and ***allometry*** of form, as well as accurately characterizing small structural details. Like other research into 3-D cranial data analysis, this research is testing the suitability of 3-D surface data for determining the sex of an individual by introducing a method of direct measurement to quantify a method that has been successfully applied as a qualified craniometric assessment of sex (Graw et al. 1999; Walker 2008; Shearer et al. 2012), specifically the upper lateral orbital margin. Previous work has shown that the mid-facial area that includes the left and right orbital torus, orbital margins, superior orbital plates and the lateral structures of the frontal and zygomatic bones is sufficiently dimorphic in adult crania to classify individuals in a sample population by sex. Of the traits of the structures described above, the transition of the upper orbital margin between the orbital torus and superior orbital plate is measured qualitatively for the purposes of

coordinate and linear craniometrics (Walker 2008). Qualitative measurements, such as Walker (2008), are subjective to the observer. Although a trained and experienced observer would be expected to produce consistent observations, two or more observers could still produce observations that differ. As long as the aspects and dimensions measured are consistent and homologous, directly measuring traits quantitatively should result in less subjectivity and inter-observer bias. Digital environments should prove beneficial for the development of quantitative measurements once challenges that stem from the segmentation of complex and variable biological structures can be consistently controlled. Pinto et al. (2013) approach the problem by segmenting an area of the orbital margin by proportional functions of height and entropy that this region is suited to by structural nature. That is to say the area is separated from the cranium and quantified by the degree of deviation from a flat plane that divides the section and bases the calculation of height as difference from the flat plane. The surface variation of the region separated by the plane (entropy) is quantified by the degree of deviation of ***normal*** vectors from the singular direction of a geometrically defined flat plane.

The negative aspect to the method employed by Pinto et al. (2013) has to do with an unclear definition of the segmentation of the sampled region of interest and disassociation with the global homology of the remaining cranium. The method used has problems with uniformity in application and replication of the segmentation of the ROI for other researchers. Segmenting out a lateral structure and aligning all individual observations from a sample runs the risk of obscuring variations that are due to the orientation of the structure within the greater super-structure. Since they apply an alignment on the ROI that changes the orientation of

each sample to minimize the variation ***Generalized Procrustes Alignment (GPA)*** each sample can be disassociated with the original cranial orientation. Some variation intrinsic to the individual could be lost by the application of this type of alignment

Ross and Williams (2008) disagreed with the application of GPA to analyze the differences in sample orientation that were a factor of the inter-observer differences in the orientation of sampled crania. Rather than align the models using GPA, the authors determined to use inter-observation inter-landmark distances to characterize each individual in the sample. This did essentially ***discretize*** the skull into a series of linear measurements, but it prevented the loss of information about the observer differences in the sample that would have been factored out as a process of GPA. The use of all distances between all points was also employed by Ercan et al. (2008) to assess observer variation in landmark position.

Ross and Williams (2008) tested the significance of the between observation variation under mixed ANOVA applied to data collected with the criterion method used for this analysis. Application of this method to this experiment uses the error, defined as the proportional difference (REL) between the process ILD observation and the criterion ILD observation factored by the process, the primary terminal point, and the ILD. This test indicates the variation overall by process and subject to noise from particular ILD.

It is possible, as shown by Ross & Williams (2008) and Ercan (2008) to align a series of multi-dimensional measurements without the scaling and rotation that takes place with GPA. The method that will be applied in this thesis is described by

Morpheus et al. (Slice 2013) software and documentation as a ***Bookstein Alignment***. This method requires two starting points to be aligned to the x-axis. The first will be set by translation - shifting the values of the y- and z-coordinates to zero (0) and subtracting the original value of the y- and z-coordinates from the values of all other y-and z-coordinates for all points in the model (this can be done with mesh ***vertices*** as well). The second starting point is aligned to the x-axis next, which involves rotation around the first point, which shifts the values of the y- and z- coordinates to zero (0). The actual geometric distance that all other points in the model will move by rotation varies by distance from the origin, but the degrees of rotation in the y- and z-planes do not. Applying rotation to all points does not disrupt the relationship of the points to each other. The last step is for three dimensional data and involves a second rotation step that uses a third point which is rotated onto the x-plane and causing the x-coordinate value to shift to zero (0). The transformation matrix is the map of the process of this re-orientation that indicates the translation and rotation of the origin into the new spatial orientation. Once all models have applied the transformation matrix that orients them to the same x-axis and z-plane, they can be translated to a common origin by selecting any coordinate (origin') and subtracting the x-, y-, and z-coordinate values of the selected coordinate common (origin') from the x-, y-, and z-coordinate values of all other coordinates for each model. This will result in all models in a sample sharing origin and alignment in three dimensions without any change to individual model geometric relationship. This method accomplishes a type of model ***registration***. Although other methods exist to accomplish an aligned registration of data or

models for analysis, the above described method is selected for the purposes of transparency.

The general system under which Geometric Morphometrics (GM) has developed is influenced by the work of Lele and Richtsmeier (2001), which outlines challenges of researching structural data. The authors propose that process in which the original orientation of data points is modified, the statistical validity of the variance of the distribution of the data is made unreliable. With few landmarks having an undefined or unstable relationship between them, orientation creates a definition that supplies a stability so long as it is either not changed, or all changes are applied universally to all subjects. As this concern is related to the maintenance of the original orientation of a sampled object as part of the definition of the location of a point and to permit the continuous identification of a landmark, it is considered and set aside as a strict interpretation. The cranial landmarks selected for the purposes of this study are individually, and as much as possible, sequentially identified. The labels and sequence conserve the spatial relationship of the points so long as any transformations are equally applied. For the purposes of assessing the statistical relationship, this project does adopt the use of ***Euclidean distances*** to address similarity for the sake of having an orientation insensitive factor for analysis. This addresses the concern over loss of comparative statistical validity of translated data having an unstructured or contrived geometry such as a set of triangles or a small number of landmarks in a multiple species sample. The sample here represent multi-dimensional coordinates of a single species sample with identified landmarks and as such will be presumed to overcome this issue for the purposes of this project where it would present a potential challenge. To study

the relationship of the landmarks derived from the four processed models without reducing the comparison values to their Euclidean distances would be preferred, if it was computationally practical. As it is not, the landmark variation is considered by two separate analysis; the ILD distances between all unique pairs of landmarks for each sampled crania, and the Point Variation of each sampled point from the processed models and Microscribe® (Revware, Raleigh, NC, USA) digital sample. If this project were to only consider the variation of the landmarks individually, the conclusions might be subject to the unreliability Lele and Richtsmeier (2001) specifically coach against, having a lack of spatial coordinate conservation and not accounting for causes of variability between the individuals of the sample and the impact on variation between processing methods.

Reporting on 3-D modeling technology for paleontology, Smith and Strait (2008) undertook testing of systematic scan data collection of mammal dental materials. A focus of the project was to examine error between materials and models, and models between cast generations. The authors introduced an error factor to their digital models by using a surface treatment of chemical *whiting* ammonium chloride, which is a well-documented technique used first to improve photographic capture of objects. The process adds slightly to the volume of the surface, but overwhelmingly improves the capture quality of laser scans on refractive surface by reducing the amount of noise incorrectly processed by the sensor. This is the type of consideration to be made for the utility of 3-D capture and analysis for anthropology discussed by Cignoni et al. (2008) in a cultural heritage context. The authors point out the necessity for careful consideration of scan preparation, acquisition and processing parameters. This speaks to the

importance of having researchers who have a good background to understand the factors that impact the collection and processing of 3-D scans.

Descriptive systems have been used due to the complexity of biological forms, and the difficulties presented with direct quantification. These methods include those of Walker (2008), Buikstra and Ubalaker, and Suchy and Brooks (white and Folkens 2000). 3-D modeling has the potential to offer quantification and systematized measurement of complex traits and forms. This fact has not been ignored by researchers. Garvin and Ruff (2012) considered quantitative adaptations of methods of sex determination based on multi-dimensional morphologies of the chin and browridge. Their study of the chin built on the approach of Thayer and Dobson (2010) using mathematical principles that result in statistically testable results. Sholts et al. (2011b) went further by testing group affinity, which is derived, for their purposes, from a suite of mid-facial structures.

In an earlier study, Sholts, et al. (2010) considered aspects of 3-D model resolution for the impact on surface area and volume rending of meshes with different sizes of "triangles". The cranial models under investigation were processed to have resolution by triangle area of 0.34 cm and 0.11 cm. While the study concluded that there were detectable differences between the two different renderings, these differences were not significantly different for the purposes of craniometric study. The authors also concluded that computational constraint prevented the use of models having the highest possible resolution given the scanning equipment employed.

Digitizer data, technology and history within biological anthropology

Human observation and landmark recording of digital models has a variable margin of error that can be influenced by differences in visual presentation that could vary with hardware and software and experience. These potential sources of variability contribute to the differences between handling actual bone remains, and remote study. Thus far, the accepted assumption is that the error from digital capture methods is mathematically small, but differences could increase in magnitude at every stage between capture and final model (Ross and Williams 2008; Smith and Strait 2008; Sholts et al. 2010).

The methods undertaken in this project do not discount the arguments presented by Lele and Richtsmeier (2001), or the methods of Ross and Williams (2008) and Ercan et al. (2008) those arguments influenced. The two samples used in this thesis allow this project to be considerate of the influence that the location of an individual landmark point or definition of a landmark point might have on the variation between multiple observations and further on the influence variation between observations could have on the measure of the linear relationship between landmark points singularly and throughout the coordinate system. As an example, Type III landmarks are defined in terms of a structural or geometric dependency. Variation in the dependency would result in variations in the terminal definition of the landmark location. When a highly variable landmark is a terminal point of an inter-landmark distance, that variation will have an influence on the ILD variation for all distances that include the Type III landmark (Ross and Williams 2008). At the same landmark, an experienced observer would be expected to show consistency in selection of a landmark even in the case of a highly variable

landmark. If that consistency prevents the conclusion of statistically significant differences, then such a variable landmark would not contribute to a rejection of the null hypothesis.

All the traits under study in the research described here are difficult to measure directly, and therefore the successful application of quantification procedures allows for conclusions that should not vary based on the scale or experience of the researcher. 3-D Landmark data (Microscribe® (Revware, Raleigh, NC, USA) and Polhemus digitizers) have a history and are accepted tools of applied 3-D coordinate analysis within biological anthropology (Ousley and McKeown, 1999 (Ousley and McKeown 2001)). This was the first technology to allow for the retention of relative landmark relationships in 3-D in addition to ILD and chords which characterize traditional craniometric analysis. Data collected with a digitizer can be composed of individual points and scribed curves (or arcs as referenced in 3Skull 2.0.171(Ousley, 2010) (Ousley 2010) and applied by Williams and Slice, 2010 (2010)). Comparatively, digitized data is dimensionally advanced over two-dimensional craniometrics; however it is still a reductive method of data collection, simplifying the crania into a series of homologous landmarks and/or curves. Areas lacking in homologous landmarks are poorly represented by this simplification (Klingenberg 2010). Euclidean distances calculated from 3-D digitized point data do have the advantage of being proximate to the caliper-based two-dimensional craniometrics that were used before the advent of digitized methods and continue to be taught and used to date where equipment for scanning and digitizing are not available. Training and experience have an impact on the relative accuracy of the collected data, and a trained observer should be sensitive to

variations in homology between individuals and populations. Reliability of digitized landmarks, and comparing landmark selection in direct and digital environments have been addressed by researchers in medical and anthropological fields (Slice et al. 2005; Olszewski et al. 2006; Olszewski et al. 2007; Olszewski et al. 2008; Ross and Williams 2008; Wong et al. 2008; Olszewski et al. 2010; Ross et al. 2010; Sholts et al. 2010; Sholts et al. 2011a; Sholts et al. 2011b; Shearer et al. 2012; Jantz et al. 2013; Olszewski et al. 2013; Abdel Fatah et al. 2014; Hale et al. 2014). For these experiments, collection samples are selected to attempt to control for learning and observer bias, and the authors have employed multiple observers and multiple collection sessions. Experimentally, this is an accepted framework. However, this selective process fails to address the limited and random nature of data.

Both caliper-based two-dimensional craniometric data and digitized point data have proven validity in the field of anthropometric study. However, the nature of the data they convey is limited by the reductive sample nature of landmark data. When applied to the experiments in which they are the designated data collection method, the landmarks and distances are valid. Having only the landmarks and distances, a researcher could not return to the data and ask questions about shapes and curves and features that are not represented by the collected points. Having 3-D models from which to collect simple and complex data for analysis is of greater flexibility and advantage to the researcher.

Chapter Three

Materials and methods

The primary research materials under study are three dimensional mesh models produced from 3-D laser surface scans of a sample of the crania from the 18th century burials found in the Yacchi-no-gama (Yacchi cave) site on Kumejima (Kume Island) in the Okinawa Prefecture. Scan data from the 3-D laser surface scans were managed via software into the models used in the landmarking procedure to extract data examined under the primary test of Correlation Coefficient test and the secondary tests of Analysis of Variance and Similarity of Means.

Materials

Description of the sample

The proposed data set for this project consists of digitized cranial landmarks collected via Microscribe® (Revware, Raleigh, NC, USA) and 3Skull Software (Ousley 2010) by Beatrix Dudzik (2012) and 3-D surface scans collected via Z-Scanner 800 (3DSystems, Rock Hill, SC, USA) by Noriko Seguchi (2010). The collected crania represent 18th century burials found in the Yacchi-no-gama (Yacchi cave) site on Kumejima (Kume Island) in the Okinawa Prefecture and housed at the Okinawa Prefectural Archaeology Center, Okinawa Japan. This sample has not had any selection criteria applied to eliminate individuals based on preservation, age, or sex. Individuals have only been excluded if the original scan data is corrupted.

The two sample data from this collection were drawn at different times. Not only was the technology used for the collecting of the samples different, the collection protocol required of the researchers was different. Seguchi (2010) applied a data collection method that required minimal contact and handling of the materials and reported few restrictions on data collection. Dudzik (2012) later reported that due to continued deterioration of the materials the collection management required the use of a thin sheet of vinyl between the sample surface and the Microscribe® (Revware, Raleigh, NC, USA) probe.

The sample under study is chosen to represent some of the important considerations for craniometric study that can be facilitated by the use of 3-D models. The full sample includes both Microscribe® (Revware, Raleigh, NC, USA) data points collected directly from the crania and 3-D scan data that has been used to produce virtual digital models. With these two types of samples, correspondence by correlation of virtual digital models with direct measurements can be tested.

The depositional environment of the southernmost islands of Japan is tropical, which is regarded as highly destructive with regards to bone preservation. This climatic consideration makes cave burials a valuable resource for the study of past populations. This collection is cared for under the auspices of a foreign government agency, which is effectively a gatekeeper to data collection as well as the future of the collection in terms of curation and preservation. To have a digital collection of materials in reasonably good condition overcomes many barriers to the study and understanding for the human history of Asia.

It has been suggested since the first part of the 19th century that the populations inhabiting the Okinawa Island chain are distinct from the populations of the Japanese Archipelago and the other regions surrounding the East China Sea to which it is adjacent - the Central China Coast, the Southern Korean Peninsula, and Taiwan (Fukumine et al. 2006; Moiseyev 2009; Consortium et al. 2012; Fukase et al. 2012). These suggestions propose that the particular characteristics of the Okinawa Island populations - and the Ryukyu Kingdom that was the recorded historical culture of the southern Okinawa Islands - were attributes connecting the populations to the pre-Yayoi (Iron Age) Jomon Culture. Over the intervening time, various investigators have undertaken research to bolster or refute the suggestion of a Jomon ancestry (Fukumine et al. 2006; Koganebuchi et al. 2012). Before the advent of ancient DNA studies, and in the absence of sufficient ancient DNA samples, studies of cranio facial and dental characteristics have relied heavily on qualitative analysis of scarce samples. Saso et al. (2011) is an exception to the qualitative trend as discussed in a previous section.

It is rare that a researcher in the field would collect and average more than one or two repetitions of landmark collection on the same individual. There is also no way to control for the conditional nature of human crania that have survived the circumstance of their taphonomic environment. The result is important typological and reference materials that can be severely compromised compared to large forensic collections. Envisioning a future of anthropometric research in which it is more common to study materials remotely in a purely digital or a digital reproduction form, the chances that all research pertaining to a sample will be undertaken by an original observer would be unlikely. There are many advantages

to the use of digital models to be explored, but importantly, such methods permit the study of materials to be undertaken regardless of distances between collections and researchers without putting the preservation of materials to further risk of damage due to handling.

Methods

Two processing parameters are used crosswise to produce four models; two with a large number of ***vertices*** and ***faces*** distributed over the whole model, and two contrasting models with fewer vertices distributed to concentrate points and faces to areas of greater complexity, each pair differing by ***manifold*** state, an open or closed geometric state of a mesh model (Cignoni and Scopigno 2008;Jantz et al. 2013; Abdel Fatah et al. 2014).

Validity of the 3-D coordinates for **Landmark Point Variability**; the landmark variation for each processing method, is assessed as the degree of correlation between the Criterion landmark point and the corresponding point of each of four processing models

Validity of the linear distances for **Paired Inter-Landmark distances (ILD)** of coordinates for each processing method is evaluated as to how closely the linear distance selected from 3-D surface scans indicate statistical correlation with the linear distances of the digitized point data for the distance between all unique pairs of landmarks.

In this case, the directly collected landmarks and original 3-D scans have been collected essentially blind. The scans and landmarks were collected by two

outside contributors offering very limited feedback and sample description of the crania of the original direct samples.

The measurement construct of craniometrics derived from Cartesian landmarks directly collected in three dimensions represents an established criterion method against which the validity of the use of craniometric Cartesian landmarks derived from multi-dimensional models in a digital environment can be tested. Assessing the correlation of the landmark variation under the processing levels proposed here establishes the presence or absence of concurrent validity of the data collected and processed in the digital environment to the data collected directly from a physical specimen.

The processing methods result in four models that represent all combinations of each of the two levels of process parameters. The first set of process parameters is analogous to resolution of an image. 3-D mesh models are built from vertices interconnected to form faces. As the number of faces increases, as with image resolution, the mesh of a 3-D model appears smoother. Two levels of *resolution* have been chosen to represent the potential impact of the number of faces (and vertices) on the selection and location of landmark points. The second set of process parameters involves possible geometric states that virtual models can exist in so long as they are in an exclusively digital environment. A mesh model built from a 3-D surface scan is not a true geometric solid. As an example, a sheet of paper represents a true geometric solid. It could be thought of in general as having a front and a back, from the perspective of 3-D geometry a sheet of paper has an outside surface and internal material in between. Even if a hole is punched through

a sheet of paper, walls of the hole will maintain the outside surface and the solid state of the sheet. In virtual 3-D rendering of a mesh model, a mesh will have an outer surface and an inner surface. The outer surface need not be complete or continuous to be rendered in a digital environment. Such a mesh model is defined as non-manifold and can include models having overlapping, non-coincident (surfaces that overlap but do not touch or meet smoothly). Most software used for the manipulation of 3-D mesh includes protocols to make a mesh model continuous and remove or repair any overlapping surfaces. Depending on the settings used, the mesh can be further made *watertight*, which repairs any places an incomplete mesh has a hole that exposes the inner faces. The results of the application of a watertight manifold process is an effectively solid model and the process is a requirement for a mesh model that will be used in and additive reproduction - such as 3-D printing, or Computer Aided Manufacture (CAM). The 3-D mesh models used in this thesis were processed to result in sets of models that were non-manifold and sets that were watertight manifold.

The two levels of each process parameter applied to the sample results in four sets of 3-D mesh models referred to by the combination of process parameters each set represents.

Strong correlation of one or more processing parameters should indicate that the landmarks derived from strongly correlated process models are valid as representations of the criterion direct digital landmarks and further, the physical crania.

Weak correlation of one or more processing parameters should indicate poor convergence and suggest that the process model whose landmarks have low correlation vary from the criterion method in some significant way.

Although the results of this validity testing will apply specifically to the sample under examination, the experiment was designed to take into consideration generalization to different 3-D and traditional data collection methods as samples become available. The processed Yacchi 3-D sample (Seguchi 2010) will be made available for analysis to future researchers. The unique nature of the sample is significant, but practical concerns to collecting a new sample from the skeletal materials onsite would prove prohibitive. The amount of complexity that can be imparted to data by making use of 3-D scans informs the utility of a thesis such as this. It is a concern for the purposes of future applications of this type of data set that uniform processing methods are tested against known standards of analytical metrics. This type of study is a primary step in understanding the consequences of digital data collection and processing on samples that are traditionally only studied directly.

Model Processing

Preparation

The raw scan data for each cranium contributed by Seguchi (2010) must be processed to clean, align, and merge the superior and inferior views taken during scanning. Once merged, the scans can be further processed to remove extraneous data and correct scanning errors. At this point, the ***manifold*** version of the model will be made which will produce a geometrically solid (or watertight) object.

Although the non-manifold models could not be rendered to a physical reproduction method, such as 3-D printing, the landmarking process does not require that a model be manifold. Further, each landmark collected will have a ***normalized vector*** perpendicular to the surface it defines.

From the manifold and non-manifold scan models, tertiary processing will be applied to create a sample set from each cranium of a research model for each of two processing criteria: high-face count, and low face count. The target number for faces is 150,000, determined by the mean number of faces of the primary models after the manifold step. The target number of faces used for the low face count models is 50,000 faces (Jantz et al. 2013). Landmark collection follows the suggestions of Jantz et al. (2013) and Hsiao (1996) using selection planes that orient with the Frankfurt Horizontal Plane, and the Mid-Sagittal Plane to determine midline and lateral landmarks by their geometric description. The location of remaining landmarks lacking a geometric location will be determined and refined by visual assessment.

Initial Cleaning

The Z-Scanner 800 is a handheld surface scanner. With this application of scanning technology, the scanner is moved by the operator over the surface of interest which is ideally static in position throughout the capture pass. The Yacchi-no-gama crania were placed on a ***calibration surface*** and scanned in two passes (superior and inferior) for each of the cranial and mandibular elements. Original scans include some areas within the scan environment that were not part of the skulls which were captured in the scan passes. This is a normal by-product of

scanner interaction with the immediate scanning environment and can be advantageous when the extra scanned areas serve to calibrate and improve the alignment of the scan model. After a scan is captured, the unwanted areas can be removed from the mesh file produced by the scanner.

Meshlab software (Cignoni et al. 2008) was used to select and delete the unwanted areas from mesh files of the superior and inferior cranial scans. The resulting mesh files were reformatted into *.ply (polygon file) format.

Merged Models

The superior and inferior components of the models were aligned by common geometry manually selected by the observer. After this initial alignment, the Meshlab software (Cignoni et al. 2008) is directed to process the two components into an alignment with as small a distance squared error (d^2) between overlapping components. Low d^2 is preferred. After alignment the d^2 average for all models was 0.062127. The d^2 for individual models in listed in Table: 4.

With the maximum alignment of the two mesh achieved, the two files can be *flattened* into a single mesh file. The flattened file retains the locations of all faces and vertices of the parent files. This can result in the retention of mesh defects. Defects can include isolated faces, unreferenced vertices, faces with inverted normals, and layers of mesh that overlap but do not intersect. These are problems that can result in a greater computational expense for analytical purposes and errors for placement of landmarks should the location intersect with a defect. Working with a large model file also affects research design by imparting a higher computational expense due to the file size. The rendering process used to project

the visual equivalent of a 3-D model in a digital environment must process large subsets of data within a single file as rapidly as possible, and without processing conflicting or corrupted data (Jantz et al. 2013).

Table 1: Computational Characteristics of Raw Models.

	Model (*.STL)	Original Pre-Process			
		File size (MB)	*Faces*	*Vertices*	*Aligned (d^2)*
1	2go-2-2_male.stl	7.1	135697	70418	
1	2go-2-2_male_bottom.stl	6.5	147960	79540	0.057746
2	6go-6-6-male.stl	6.4	134594	70825	
2	6go-6-6-male_bottom.stl	Does Not Exist - Scanning Error			
3	8-14_female.stl	6.2	123650	64925	
3	8-14_female_bottom.stl	5.9	129667	69775	0.076798
4	11-5_male.stl	6.6	136570	71262	
4	11-5_male_bottom.stl	6.5	137711	74563	0.07672
5	11-14_female.stl	6.6	130134	67908	
5	11-14_female_bottom.stl	6.2	137400	73444	0.050739
6	11-15_male.stl	6.8	144021	75325	
6	11-15_male_bottom.stl	6.9	141576	75868	0.056846
7	11-42 female.stl	7	132567	69385	
7	11-42 female_bottom.stl	6.3	147235	79105	0.068469
8	2go-2-30_male.stl	7.1	139009	72261	
8	2go-2-30_male_bottom.stl	6.6	148492	79542	0.048818
9	2go-2-32_male.stl	7.4	140304	73605	
9	2go-2-32_male_bottom.stl	6.7	155535	83869	0.078066
10	7-12-male.stl	7.5	147997	77974	
10	7-12-male_bottom.stl	7.1	158047	84722	0.075532
11	9-15_female.stl	6.2	122513	64651	
11	9-15_female_bottom.stl	5.8	130734	70120	0.047501
12	11-34_male.stl	6.4	129156	67650	
12	11-34_male_bottom.stl	6.2	134123	72795	0.063547
13	11-42 male.stl	6.7	139581	72888	
13	11-42 male_bottom.stl	Does Not Exist - Scanning Error			
*	11-19_female.stl	6.5	133777	69530	
*	11-19_female_bottom.stl	6.4	136790	73952	0.06423
*	2-13_male.stl	6.5	135489	70927	
*	2-13_male_bottom.stl	6.5	136831	74041	0.053619
*	2-16_female.stl	6.6	135939	71035	
*	2-16_female_bottom.stl	6.5	138288	74570	0.051141
		File size (MB)	*Faces*	*Vertices*	*Aligned (d^2)*
	Mean for sample	6.58	138046.2	73215.83	0.062127

* Some Model files failed to resolve during this stage of processing due to indeterminate file corruption of the source file.

Refining and aligning the raw scan files results in pre-process models which have large areas of overlap that is redundant to the model and keeps the mesh file size large. The average files size for each half of the raw scan files is 6.58 MB. Large files are undesirable because they slow down rendering and the application of any selection or analysis.

Processing the models produced two sets of two mesh models each. The processed models a reduced in size compared to the original raw scan files. The average size for the merged and processed mesh file is 2.3 MB, which is a reduction of at least 25% for each cranium. The high face count models for each cranium are larger on average, but still within a reasonable range for maintenance of detail contrasted to computational expense.

Process Levels

After the superior and inferior views have been merged, the resulting file retains the raw information of both parent files. While working with a scan that exactly reflects the surface of the source would be considered a conservative approach, to use the size of files that result from raw data models is prohibitive due to the necessary computational thresholds and added time required by thresholds.

To mitigate the issue of file size and computational efficiency, it is sensible to consider the application of mesh processing methods that uniformly reduce the file size in a trade-off that minimally impacts the retention of accuracy.

Table 2: Codes for Processes

Process	Code	Description	Parameters
hf:	**1**	**high face count, manifold**	High Face count models are processed to re-distribute the faces and vertices of the raw, aligned scans to approximately 150,000 faces and 75,000 vertices.
hfnm:	**2**	**high face count, non-manifold**	
lf:	**3**	**low face count, manifold**	Low Face count models are processed to re-distribute the faces and vertices of the raw, aligned scans to approximately 50,000 faces and 25,000 vertices.
lfnm:	**4**	**low face count, non-manifold**	
dd:	**5**	**Microscribe® digitizer data**	Landmark sample captured from the physical specimens with a Microscribe® (Revware, Raleigh, NC, USA) 3-D Digitizer

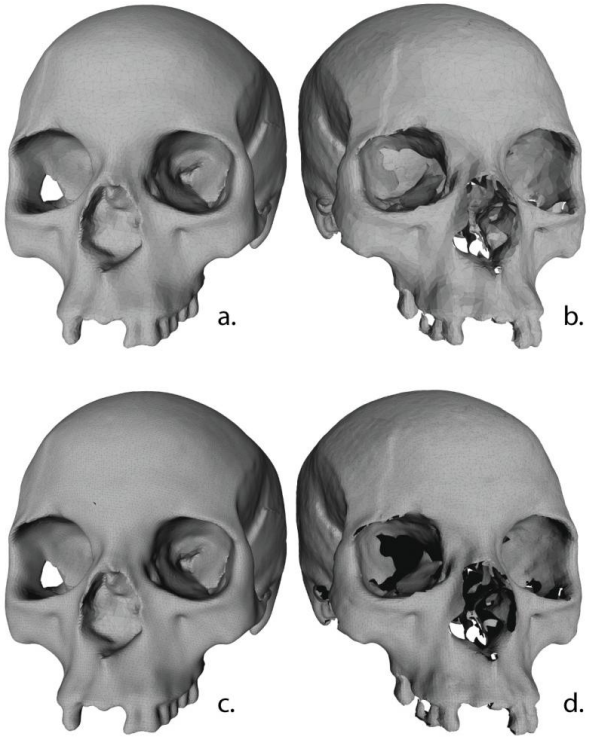

Figure 1: Examples of Processed Models

Examples of the mesh models at each of the levels of the processing parameters. a) low-face count manifold. b) low-face count non-manifold. c) high-face count manifold. d) high-face count non-manifold. Differences between the manifold and non-manifold process models can be observed in the orbital and nasal cavities and in the dental elements.

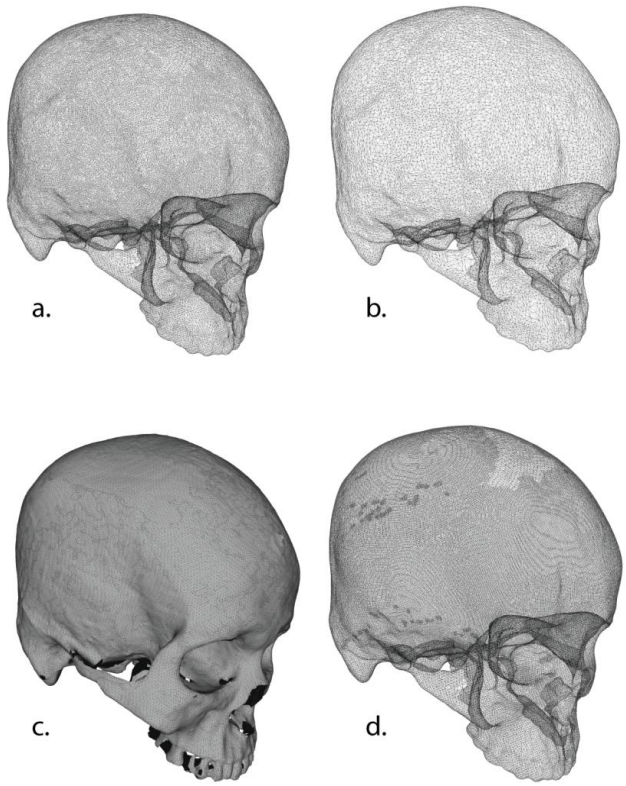

Figure 2: Examples of Stages of Processing Models
Examples of mesh models emphasizing the vertices. a) high-face count mesh. b) low-face count mesh. c) aligned, unprocessed superior and inferior mesh including the faces. d) aligned, unprocessed superior and inferior mesh. The examples c & d indicated the areas of overlap and excessive point density resulting from the scanning procedure.

Methods I use in this thesis are designed to process a 3-D mesh for optimization of file size and accuracy under either a random sampling of the surface (Kazhdan et al. 2006), or by evaluating the redundancy of the number of faces and vertices over a given area and reducing the density of both in areas and directions of low variation and maximizing the sampled density in areas of greater complexity (Hoppe 2010*).

Based on previous 3-D cranial studies of CT scans (Saso et al. 2011; Jantz et al. 2013) and surface scans (Sholts et al. 2010; Sholts et al. 2011a; Shearer et al.

2012) the processing levels analogous to resolution were set at 150,000 faces (~ 75,000 vertices) for the high resolution models, and 50,000 faces (~ 25,000 vertices) for the low resolution models.

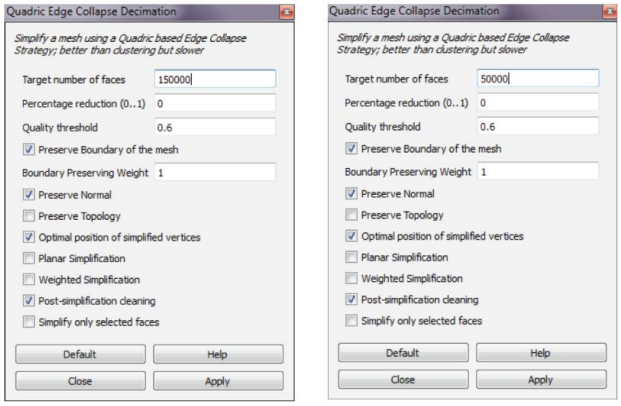

a. b.

Figure 3: Meshlab (Cignoni et al. 2008) Simplification Settings
The settings applied to the aligned and joined hemispheres of the unprocessed models to effect the (a) high face count and (b) low face count process models

Since the time Sholts, et al. (2010) was written, processes for accurately rendering 3-D meshes have improved. One such process, applied for this project applies the ***decimation*** of the mesh to the low face count mesh models to render the number of faces and vertices of complex areas more densely and non-complex areas with less density. Decimation involves the use of a quadric model that compares a single vertex or edge to those nearest and records the variation, this step is then repeated for the next nearest points, resulting in a set of points that meets the criteria of a set target number of faces and distribution to vary based on the actual variation and convolution of different areas of the mesh. Differences in the variation between a starting point and the next nearest points indicates a high

probability of surface complexity – such as bending or curving of the surface - and therefore indicates an area that would require a greater density of faces and vertices to characterize the shape of the original mesh model. Conversely, very low or no difference in the variation between the starting point and the closest points indicate a low probability of surface variation – a flat face of a cube, for example - and suggest that the area can be accurately rendered with fewer faces and vertices. The procedures for decimation implemented by the Meshlab software (Cignoni et al. 2008) as applied for this study use this quadric method with multiple iterations to develop a best fit representation of the original mesh model with a specified target number of faces. There is an advantage of multiple iterations in that the potential for every seed, or initial starting point used for each iteration, having a very high or low complexity relative to the overall mesh and exerting a strong influence that introduces bias to more distance parts of the mesh is minimized. (Hoppe 1999). Once this has been applied, the areas of the "triangles" over the mesh vary greatly depending on the degree of change over the surface at a given area of the mesh.

Standard Alignment

Orientation differences between 3-D digitizer coordinates, CT Scans, and surface scanning technology present an issue regarding inter-operability is the capturing orientation. It is possible to orient a subject object for 3-D scanning in any way, although consistency is recommended for multiple scans if for no other reason than the researcher’s a priori knowledge about the object. Orientation is important to geometric of data because significant differences in orientation can

lead to weak statistical conclusions at the time of analysis if they have not been accounted for. Lele and Richtsmeier (2001) suggest this to be due to any presumptive alignment taking place to the coordinate matrix of any set of coordinate data. This serves as a good warning against the possibility of spurious conclusions made from poorly understood or poorly aligned models. This study must be concerned with data collected by different means, each of those having slight differences in orientation. Therefore, this project must rely on the relationship between the coordinates of each set of points and each model to appropriately orient all data for the multiple process models and the Microscribe® (Revware, Raleigh, NC, USA) digitized data.

CT scans are built from 2 dimensional layers, each oriented as *(X, Y)* and building the *Z-plane* by stacking each successive layer. This is the global capturing orientation, which is parallel to the slices of a CT scan, and independent from the resting orientation of the object undergoing scans. Surface scanning and coordinate digitization both take in data in all dimensions simultaneously either dynamically or rotationally for most scanning systems. If a cranium were to be placed on a single basal resting orientation and subjected to a CT scan and a surface scan, the resulting data would produce models that divided the X, Y, and Z planes differently.

Anthropological training in the use of coordinate digitizer collection usually specifies a resting orientation of individual samples on the ***Frankfurt Horizontal plane*** (Figure 5) or resting on the basal portion of the skull. Protocol for use of a secondary orientation is documented by Morpheus, et al. (Slice 2013) to make for

an easier capture of basal or lateral landmarks within the work area of the digitizer arm. The alternative for cranial point sampling involves a flexible pedestal and mirror (Ousley 2010). Uniformity of orientation is usually considered globally consistent enough to permit comparisons of samples collected by the same or multiple identically trained observers. Observers using different resting orientations have problems making direct comparisons of landmark coordinates, as discussed in Ross and Williams (2008).

With a few exceptions, surface scanners create a dynamic orientation based on the object. Complex objects like a skull necessitate capture of multiple orientations that are stitched together as described above. If the models were to be used for direct comparison or having coordinates collected without a standard alignment, the dynamic nature of scan collection can create problems.

To solve the problems with orientation with all methods, it is practical to apply as near as possible the same alignment to all methods. Some degree of variation will still occur, as it would for different observers or on different days, so it is expected that the variation would be within an acceptable threshold. Software used to manipulate and generate 3-D models uses an *x, y, z* virtual environment to render the models. If a model is moved in the environment, the changes in linear position (translation), rotation, or scale are recorded in a ***transformation matrix***.

Models built from surface scans or CT scans can be visually oriented to the Frankfurt Horizontal plane by aligning the site of porion on the left and right lateral aspects of the cranium with the lowest point of the inferior orbital margin. From here, the mid-line can be estimated for orientation from multiple structures.

Standard alignment is applied to the cranial models by transformation matrix generated from manually transforming a primary merged model *(Alpha)* in CloudCompare software (Girardeau-Montaut 2014) as described above. The transformation matrix is saved as it can be re-applied to models of that specimen generated from the primary merged model.

Landmark Sample

Placement and recording of landmark points in a digital environment can be accomplished by any one of several available of methods. Software designed for manipulation and rendering of 3-D models typically would have some associated function for placing a reference point on a model and recording the location of that point relative to the 3-D environment to assist in registration of objects in the 3-D coordinate space. For the purposes of this project, Stratovan Checkpoint© software (Stratovan Corporation, Davis, CA) was selected because the viewing options are more advanced than other options for digital landmark point collection. This commercial software allows selection and placement of points, landmark labels, and export of the collected landmark points to several file formats. For general versatility, the *.CSV (Comma separated values) have been used to export the landmark point coordinates from Stratovan Checkpoint© software (Stratovan Corporation, Davis, CA). The use of this software for this project was granted by the makers under an extended trial directly to the author.

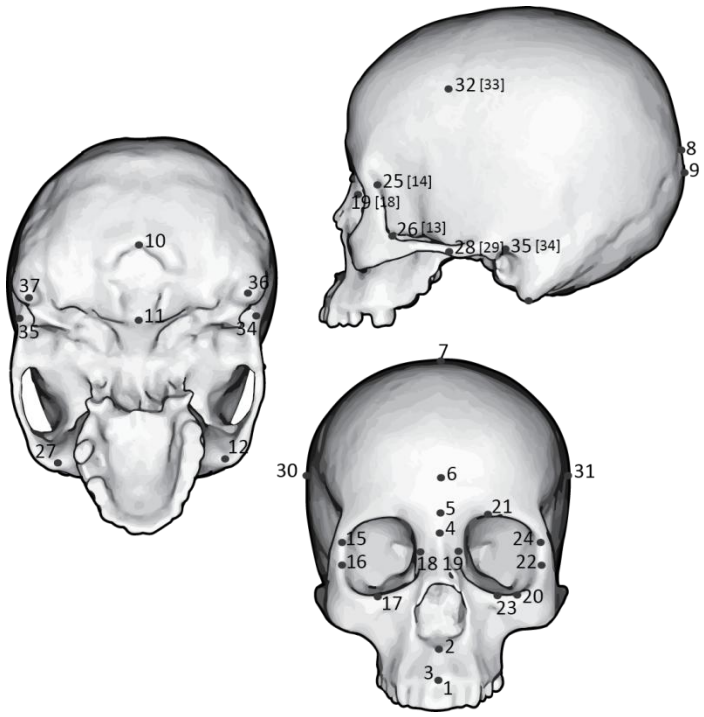

1. prosH
2. ssp
3. prosM
4. nas
5. glb
6. spglb
7. brg
8. lam
9. opg
10. ops
11. bas
12. zygomr
13. jugr
14. fmtr
15. fmar
16. ectr
17. zygoor
18. dacr
19. dacl
20. obhi
21. obhs
22. ectl
23. zygool
24. fmal
25. fmtl
26. jugl
27. zygoml
28. zygl
29. zygr
30. eurr
31. eurl
32. stpl
33. stpr
34. porr
35. porl
36. mastr
37. mastl

Figure 4: Landmark Map
Visual map of the location of the landmarks sampled.

Landmarks selected for collection and analysis for this test were required to meet several criteria (Ross and Williams 2008; Sholts et al. 2010; Saitou et al. 2011). First, it was necessary to select landmarks that had been part of the direct Microscribe® (Revware, Raleigh, NC, USA) data collection which was the derived from the ThreeSkull v.2.0 software (Ousley 2010). ThreeSkull v.2.0 is an interface used to direct the collection of digitizer points systematically and maintain consistent identification of landmarks as they are collected. The list of landmarks was reduced from this first list to satisfy several further requirements: (1) each landmark must exist on most or all crania in the sample; (2) each landmark must be visible either directly or accurate to estimate based on the 3-D mesh models with the highest resolution (high face count models). The latter requirement

disqualifies landmarks with particular definitions that require visualization of sutural intersections either smoothed (obscured) or non-smooth (bumpy) areas; or may lack adequate scan capture due to size, complexity or fragility (damage). Examples of landmarks that cannot be accurately estimated without direct visualization are ***asterion***, and superior and inferior ***zygotemporale***. The mesh models under study here were captured without texture, which prevents the visualization of these areas for selection of landmark locations. Asterion is an intersection that is found within an area of convoluted sutures between the temporal and occipital bones. The zygotemporale landmarks are not only dependent on visualization of the suture between the zygomatic arch and the temporal arch, they are also dependent upon accurate capture of the small, fragile structure.

The process of elimination based on the requirements determined above resulted in the final list of landmarks selected for the 3-D digital data collection.

Table 3: Landmarks for 3-D Comparison

	Abbrev.	Landmark	Type	Definition
1	prosH	prosthion-Howells	II	Most anterior point of the midline inter-dental, between central incisors.
2	ssp	subspinale	II	Deepest point directly inferior to the projection of the nasal spine.
3	prosM	prosthion-Martin	II	Most inferior point of the maxilla on the midline, between the central incisors.
4	nas	nasion	I	The intersection determined by the sutures between the frontal and nasal bones.
5	glb	glabella	III	Anterior projecting extrema of the midline of the frontal bone proximal to the orbital torus.
6	spglb	supraglabellare	III	Convex midline point superior to glabella on the midline of the frontal bone.
7	brg	bregma	I	Intersection of the coronal and sagittal sutures between the frontal and parietal bones.
8	lam	lambda	I	Intersection of the sagittal and lambdoidal sutures between the parietal and occipital bones.
9	opg	opisthocranion (GOL)	III	Posterior extrema of the crania on the midline.
10	ops	opisthion	II	Most posterior point of the foramen magnum on the midline.
11	bas	basion	II	Most anterior point of the foramen magnum on the midline.
12	zygomr	zygomaxilare R	III	Inferior extrema of the suture between the zyogmatic and maxillary bones
13	jugr	jugale R	II	Deepest point (anterior) of the transition between the frontal and zygomatic processes.
14	fmtr	frontomalare temporale R	III	Posterior extrema of the suture between the frontal and maxillary bones.
15	fmar	frontomalare anterior R	III	Anterior extrema of the suture between the frontal and maxillary bones.
16	ectr	ectoconchion R	III	Most lateral point of the margin of the ocular orbit.
17	zygoor	zygoorbitale R	II	Location of the zygomaxillare suture crossing the margin of the ocular orbit and the inferior orbital plate.
18	dacr	dacryon R	II	Alternate definitions place at the sutural intersection of the lacrimal, maxillary, and frontal bones -or- the apex of the lacrimal fossa. The definitions may be concurrent, or indeterminate depending on the individual.
19	dacl	dacryon L	II	
20	obhi	lower orbital border L	III	The most inferior point of the margin of the ocular orbit.

21	obhs	upper orbital border L	III	The most superior point of the margin of the ocular orbit.
22	ectl	ectoconchion L	III	Most lateral point of the margin of the ocular orbit.
23	zygool	zygoorbitale L	II	Location of the zygomaxillare suture crossing the margin of the ocular orbit and the inferior orbital plate.
24	fmal	frontomalare anterior L	III	Anterior extrema of the suture between the frontal and maxillary bones.
25	fmtl	frontomalare temporale L	III	Posterior extrema of the suture between the frontal and maxillary bones.
26	jugl	jugale L	II	Deepest point (anterior) of the transition between the frontal and zygomatic processes.
27	zygoml	zygomaxilare L	III	Inferior extrema of the suture between the zyogmatic and maxillary bones
28	zygl	zygion L	III	The lateral extrema of the zygomatic arches.
29	zygr	zygion R	III	
30	eurr	eurion R	III	The lateral extrema of the greatest cranial breadth.
31	eurl	eurion L	III	
32	stpl	stephanion L	I	Intersection of the coronal suture and the superior temporal line (ridge caused by the temporal fascia attachment).
33	stpr	stephanion R	I	
34	porr	porion R	III	Point superior to the external auditory meatus, also may be determined by the posterior root of the zygomatic arch.
35	porl	porion L	III	
36	mastr	mastoideale R	II	Inferior extrema of the mastiod process.
37	mastl	mastoideale L	II	

See Figure 4 for locations. Colors are used as visual cues to group the lateral landmarks for data collection and maintain the collection index. See Appendix 4 for data collection protocol. (Howells 1973; Howells 1996; Bookstein 1997; White and Folkens 2000). In the text; *landmark* refers to a definition of a location, *point* refers to a sample coordinate of a landmark.

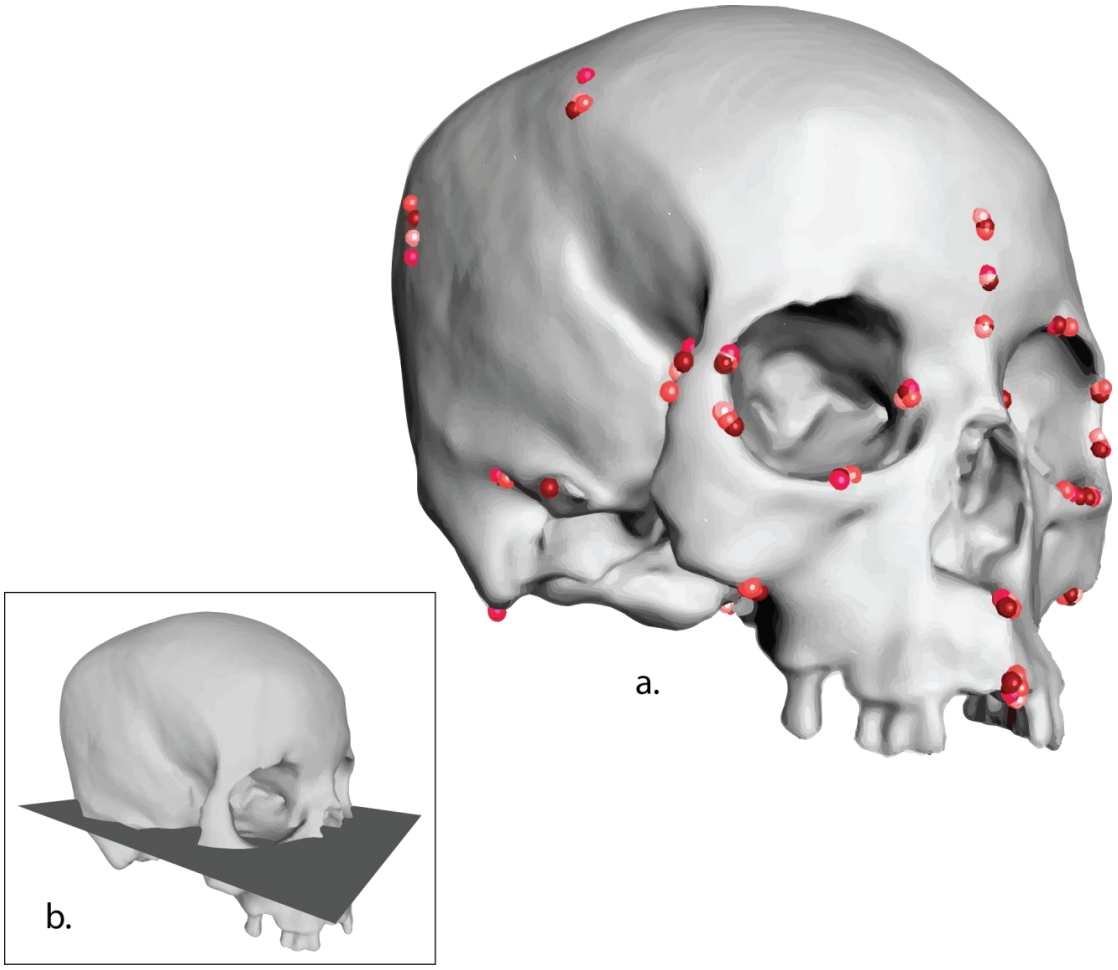

Figure 5: Example of Landmark Point Sample
This figure shows the scatter of the landmark points from all process models. In the inset, a plane indicates the Frankfurt Horizontal intersecting the left and right porion landmark points and the left zygoorbitale landmark point.

The final 37 landmarks are present on most crania in the sample and remain after the application of processing parameters for all models. These landmarks primarily characterize the global structures of the crania and structures of the cranio-facial area that are stable. Stable in this context refers to structures being present in high frequency and exhibiting low frequency of damage. The term is chosen here because in this test, non-exclusion of crania due to taphonomic

damage has been determined to be an important factor for the application of 3-D research methods using historical specimens. There is an increasing risk of error when the sample under study is small and experiences damage or deterioration. However, given the significance of historical samples in the record of the moments and the eras of human history, that risk should be considered and accepted. One advantage to the use of 3-D models is the ability to virtually reconstruct damage and deformation. Once we have a solid grasp on the potential impacts of these types of error, we can inform the methods by which reconstructed forms are imputed from the available data (Weinberg and Kolar 2005; Jantz et al. 2013).

Landmark Data Format

Landmark points for the observations of the 3-D models of that sample crania at all levels of processing was collected using Stratovan Checkpoint© software (Stratovan Corporation, Davis, CA). The output of listed and landmark labeled point locations was exported to comma-separated values (*.csv) format text files using the internal functions of the program. Due to the differences in the technologies used to collect the experimental and criterion data, the sets of points representing each cranium have different orientations in the coordinate system.

For testing the correlation of the Inter-landmark Distances (ILD), the orientation within the coordinate system is immaterial once EDMA is applied to the samples. For the purposes of the Landmark Point Variation (LPV), the differences in orientation and alignment of the samples for each cranium add a significant degree of noise and error that are best minimized. To account for the differences in original coordinate orientations between the collected 3-D model samples and the direct

collected sample, the models were aligned to a standard alignment within the coordinate system by the Frankfurt Horizontal Plane (FH).

The FH was operationally defined as the plane intersecting the right and left porion landmark points and the left zygoorbitale in accordance with the standard accepted definition. For registration to a common origin, standard coordinate system, and to the coronal and sagittal planes, which define the Y and Z planes respectively, the points must be translated and rotated to orient the left and right porion landmark points to Y and Z values of zero (0) and X values that equilaterally split the Euclidean distance between the two points. It must be stated that there is a consequence of this registration for the landmark points used to define the orientation. The multi-dimensional variation of the three is reduced such that left and right porion points only vary in X values, and zygoorbitale only varies in X and Z values. This does not significantly reduce the analytical validity of the data as the changes to the vector matrix of the points do not lose orientation relative to each other.

To effect the aligned orientation between the landmark points collected in the Stratovan Checkpoint© software (Stratovan Corporation, Davis, CA) and those collected using the Microscribe® (Revware, Raleigh, NC, USA) each set of landmark points for each crania in the sample were entered into a text file formatted for use with Morpheus et al. (Slice 2013) software with each point matched for serial position in the list of landmarks for each example.

Within Morpheus et al. (Slice 2013) software the points are processed with a three-dimension Bookstein alignment, setting an origin (porion left), translating and

rotating a secondary point (porion right) to zero for each the Y and Z directions, then lastly rotating the third point (zygoorbitale) around the X vector to zero for the Y direction. To bring the points back to the correct orientation in the XYZ coordinate plane, the sign (+/-) of the X coordinates is reversed and the Y and Z coordinates are reversed.

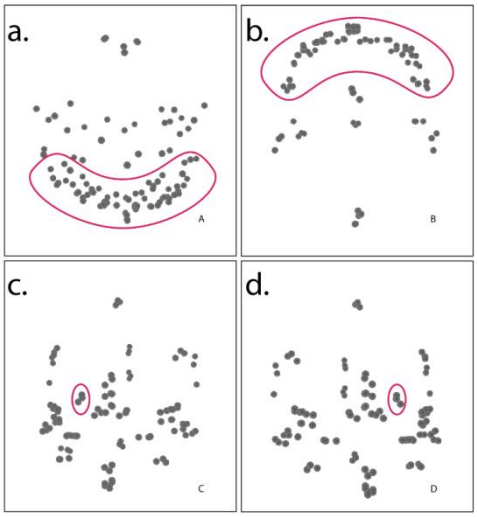

Figure 6: Stages of Bookstein Alignment
Bookstein Alignment of landmark point data allows for a set of points to be aligned to a specific subset of points, rather than a derived data centroid as with GPA. a.) The original orientation of the landmark point data imported into Morpheus, et al. (2013). Facial landmarks are highlighted. b.) The orientation after the application the Bookstein Alignment. The scatter of the points has been reduced, but the data is not aligned to the correct axes. Facial landmarks are highlighted. c.) Transposition of the data of the Y and Z axes corrects the alignment to the default 3-D orientation, but results in a mirroring effect on the data of the X axis. Left Porion landmark point cluster is highlighted. d.) Inversion of the sign (+/-) of the data corrects for the mirroring effect and completes the process. Left Porion landmark point cluster is highlighted.

Equation 1: Bookstein Superimposition Transformation - Unit - Scale (Lele 2001)

$$Obs_{Prc} = \begin{bmatrix} X_{bas} & Y_{bas} & Z_{bas} \\ X_{brg} & Y_{brg} & Z_{brg} \\ \vdots & \vdots & \vdots \\ X_n & Y_n & Z_n \end{bmatrix}$$

Obs = observation, the set of collected landmarks (n=37) from a crania in the sample

Prc = processing, the type and level of processing applied to the crania before landmarks are collected

n = the landmarks collected on each observation, also indicated by abbreviations of the location name (See Appendix)

$$Scale\ Factor\colon\ v_{(x,y,z)} = v_x = v_y = v_z = \sqrt{(X_{porl} - X_{porr})^2 + (Y_{porl} - Y_{porr})^2 + (Z_{porl} - Z_{porr})^2}$$

Scale Factor is the Inter-Landmark (Euclidean) distance value calculated between the first (*porl*) and second (*porl*) landmarks selected from an observation for Bookstein Superimposition. This process is reversed post superimposition to conserve the differences in scale between the sampled land marks for all processes and Microscribe® (Revware, Raleigh, NC, USA) digital landmarks.

$$nas = \begin{bmatrix} X_{nas} \\ Y_{nas} \\ Z_{nas} \\ 1 \end{bmatrix} \qquad Scale\ nas = \begin{bmatrix} v_X & 0 & 0 & 0 \\ 0 & v_Y & 0 & 0 \\ 0 & 0 & v_Z & 0 \\ 0 & 0 & 0 & 1 \end{bmatrix} * \begin{bmatrix} X_{nas} \\ Y_{nas} \\ Z_{nas} \\ 1 \end{bmatrix} = \begin{bmatrix} X_{nas(v_X)} \\ Y_{nas(v_Y)} \\ Z_{nas(v_Z)} \\ 1 \end{bmatrix}$$

Equation 2: Bookstein Superimposition Transformation - Plane - Rotation (Lele and Richtsmeier 2001)

Rotation factor is the degrees of rotation around the origin necessary on the *x, y* and *z* coordinate system planes to bring the second landmark (*porl*) into coincidence with the first landmark (*porl*) on the *x* plane and reduce difference of the *y* and *z* values between the first and second landmarks to zero.

$$porr = \begin{bmatrix} X_{porr} \\ Y_{porr} \\ Z_{porr} \\ 1 \end{bmatrix} \qquad Rotate\ porr = \begin{bmatrix} \cos(\alpha)\sin(\emptyset) & \sin(\alpha)\cos(\emptyset) & \sin(\emptyset) & 0 \\ -\sin(\alpha) & \cos(\alpha) & 0 & 0 \\ -\cos(\alpha)\sin(\emptyset) & -\sin(\alpha)\sin(\emptyset) & \cos(\emptyset) & 0 \\ 0 & 0 & 0 & 1 \end{bmatrix} * \begin{bmatrix} X_{porr} \\ 0_{porr} \\ 0_{porr} \\ 1 \end{bmatrix}$$

Equation 3: Bookstein Superimposition Transformation - Root – Translation (Lele and Richtsmeier 2001)

Translation factor is the linear shift required to root the first landmark (*porl*) to the origin of the coordinate system, which results in *x, y,* and *z* values of zero

$$porl = \begin{bmatrix} X_{porl} \\ Y_{porl} \\ Z_{porl} \\ 1 \end{bmatrix} \qquad Translate\ porl = \begin{bmatrix} X_{porl} \\ Y_{porl} \\ Z_{porl} \\ 1 \end{bmatrix} - \begin{bmatrix} X_{porl} \\ Y_{porl} \\ Z_{porl} \\ 0 \end{bmatrix} = \begin{bmatrix} 0_{porl} \\ 0_{porl} \\ 0_{porl} \\ 1 \end{bmatrix}$$

Equation 4: Bookstein Superimposition Transformation – Correction for Standard Coordinate System

Reverse scale, swap Y and X, inverse sign for X

$$BSC(Obs_{Prc}) = \begin{bmatrix} X_{bas} & Y_{bas} & Z_{bas} \\ X_{brg} & Y_{brg} & Z_{brg} \\ \vdots & \vdots & \vdots \\ X_n & Y_n & Z_n \end{bmatrix}$$

$$Correct\ BSC(Obs_{Prc}) = \begin{bmatrix} (X_{bas}) & Z_{bas} & Y_{bas} \\ -(X_{brg}) & Z_{brg} & Y_{brg} \\ \vdots & \vdots & \vdots \\ -(X_n) & Z_n & Y_n \end{bmatrix}$$

At this stage, the sets of landmark points are subjected to Euclidean Distance Matrix Analysis (EDMA) using PAST v2.17 (Hammer et al. 2001) to output the Euclidean distances to tables of each the unique pair of points for Inter-Landmark Distance (ILD) analysis and for each process for Landmark Point Variability (LPV) analysis. Missing data is imputed by column average substitution by the software.

Equation 5: Euclidean Distance Matrix Analysis Formula (Lele and Richtsmeier 2001)

$$Euclidean\ Distance: ILD = \sqrt{(X_{porl} - X_{porr})^2 + (Y_{porl} - Y_{porr})^2 + (Z_{porl} - Z_{porr})^2}$$

Note, that this equation is the same equation applied in the first step of the Bookstein Superimposition Transformation.

For the purposes of visualizing the distribution of the LPV sample, a plot of the process model samples compared to the criterion direct digital sample was created from values derived from pooled landmark point values of the average difference between a primary process model landmark point and the remaining process model landmark points against the difference between the primary process landmark point and the criterion direct digital landmark point.

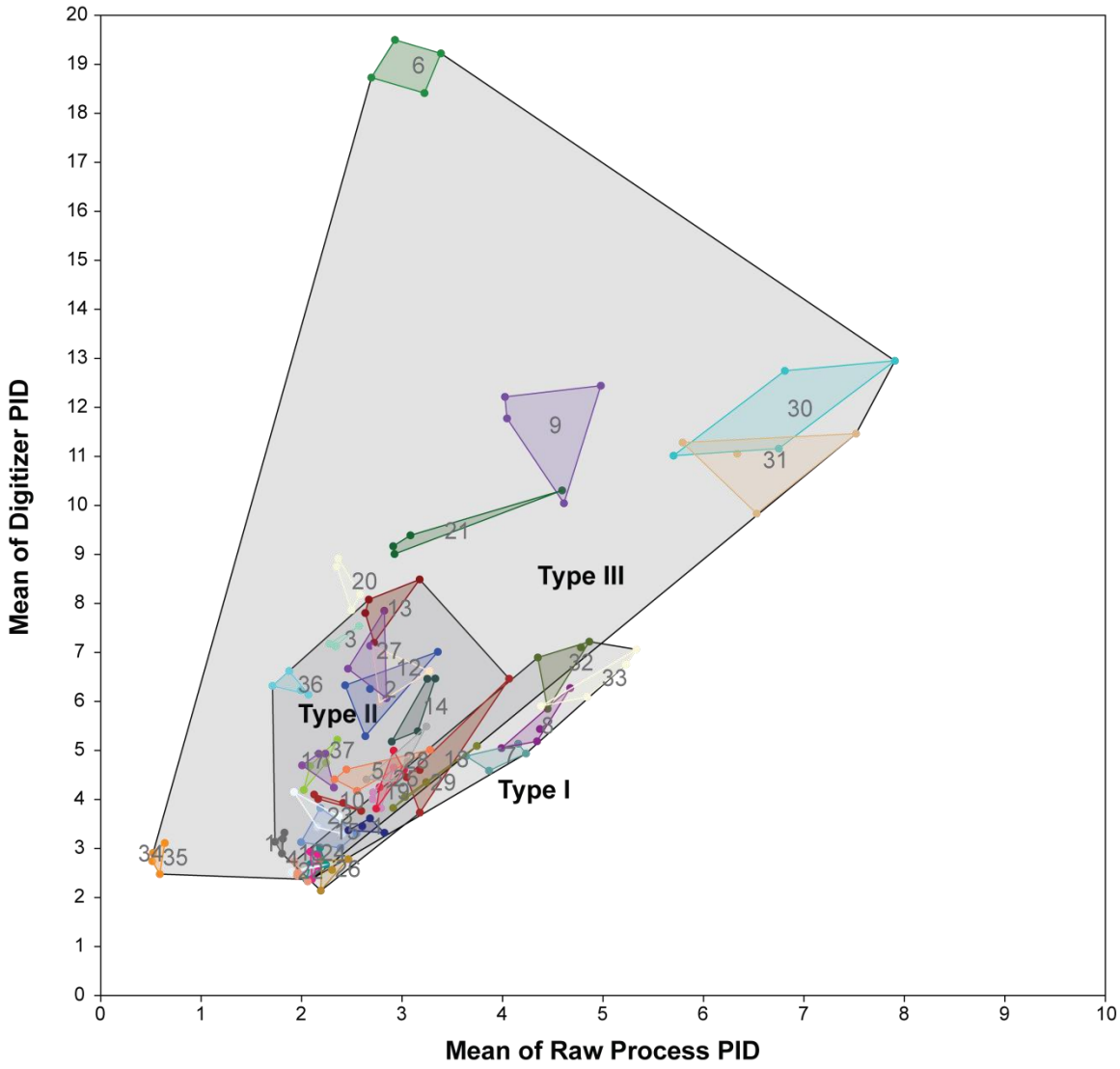

Figure 7: Landmark Point Variation Distribution

Plot of the Landmark Point Variation of all points (n=37) groups within colored polygons. Further grouped by landmark point Type (I, II, III). X-axis represents the values of the LPV for each process landmark point derived from the average of the distances of the mean of the primary landmark point to the mean of all other process landmark points. The y-axis represents the difference between the mean of each process landmark point and the criterion direct digital landmark point.

Together, the axes of this plot show the relationship of the differences of the landmark point variation of the processes and the criterion direct digital landmark point selection. Those points with the least variance between the Process landmark point selection and the criterion direct digital landmark point selection are plotted most closely to the diagonal ($x = y$).

Missing data

Coordinate points were missing from the process models sample data from eight landmark points. Missing points were the result of insufficient scan capture problems or file corruption occurring between scanning and the refinement, alignment and processing steps.

Table 4: Missing Coordinates Summary

	1. prosH	10. ops	11. bas	13. jugr	28. zygl	29. zygr	36. mastr	37. mastl
total	4	16	8	4	8	8	20	8
hf	1	4	2	1	2	2	5	2
hfnm	1	4	2	1	2	2	5	2
lf	1	4	2	1	2	2	5	2
lfnm	1	4	2	1	2	2	5	2
dd	0	0	0	0	0	0	0	0

Missing values influence rank order correlation methods. If not removed, average values are substituted with a central tendency value, resulting in an artificially high or low correlation depending on the central tendency of the sample subset.

Table 4 lists the landmark points with missing coordinates. Missing data were imputed by column substitution by the EDMA process for the ILD sample in PAST v1.93 (Hammer et al. 2001). For the LPV test, the missing values were removed for each landmark and the Mantel correlation test was applied to the reduced sample.

Statistical Analysis

For the ILD analysis, the points are tabulated by crania and unique pairs of landmark points for all processes, including the Microscribe® (Revware, Raleigh, NC, USA) digital landmark points against which the process ILD data will be compared for correlation.

Correlation is assessed for the ILD by either Pearson's product-moment coefficient of correlation r, or Spearman's rank order correlation coefficient r_s*,

dependent upon evaluation of the set of inter-landmarks distance by group (crania) for each process and for the Microscribe® (Revware, Raleigh, NC, USA) digital inter-landmark distance for normal distribution. Preliminary testing of the distribution of the sets was evaluated with the Shapiro-Wilk's *W indicating* a mix of normally and non-normally distributed inter-landmark distances.

For Landmark Point Variability analysis, the points are tabulated by landmark for each cranium for all processes. A plot of the landmark coordinate data indicated that a substantial number of the Type III Landmarks were problematic for the purposes of the analysis of correlation to the criterion direct digital landmark points. Since these problems could be examined and attributed to either observation or alignment, all Type III landmarks have been excluded from the LPV sample analysis.

Sets of coordinates are tabulated for the output for: 1.) each point for each process for all points for all crania; and 2.) the Microscribe® (Revware, Raleigh, NC, USA) digital landmark point for all landmarks for all crania. The resulting sets (n = 37 for four process models) The distance between each process point and the remaining processes were averaged to a mean value of each point by cranium for use to compare with the log distance between each process point and the Microscribe® (Revware, Raleigh, NC, USA) digital point.

The correlation of LPV was evaluated exclusively by Mantel's test (Hammer et al. 2001; Sokal and Rohlf 2011) of the correlation of the Euclidean Distance between the selected landmark points for each landmark over all sampled crania and the corresponding criterion direct digital landmark points.

The permutation method of the Mantel test method relaxes the statistical distribution requirements usually necessary to apply the Pearson's correlation coefficient used within the Mantel's test. This also overcomes concerns outlined by other studies of individual landmark point variation. These studies found alternative ways to transform the data, specifically the application of log transforms. The use of log transforms was intended to address concerns of the effect the size of differences between the landmark points selected by an observer could have on the analysis of this type of data (Olszewski et al. 2006; Olszewski et al. 2007; Olszewski et al. 2008; Olszewski et al. 2010; Olszewski et al. 2013) and to address heteroscedasticity (Wong et al. 2008).

The ILD and LPV sample sets were evaluated for random error, defined as a low degree of predictability of the values of the process model landmark points and interlandmark distances from the known criterion direct digitized landmark points and interlandmark distances. The definition of landmark points, as discussed earlier in this section in reference to the exclusion of Type III landmarks from the LPV sample analysis, is a factor that is considered as having some potential impact on correlation (Bookstein 1997). The process parameters applied to the models from which the landmark point samples are derived are considered for potential contribution to overall error.

For the ILD sample, random error was tested with the application of ANOVA, using a general linear model to indicate those points in the analysis that are highly variable to compare to the types described by Bookstein (1997) and evaluate for a the presence of error. Random error was evaluated by analysis of the distribution of

the Coefficient of Determination (r^2). This ANOVA test was done using R software and packages for ANOVA tests with a general linear model for correlation coefficients.

LPV sample was tested for the effects of random error for the same rationale as above for the ILD sample with the analysis of the Coefficient of determination (covariance, R^2) of the significant correlation of the LPV sample. Random error due to landmark point Type was less of a concern, after the removal of the Type III landmarks from the LPV sample analysis. This means the possibility of random error can be evaluated on the basis of individual landmarks impacted by correlation as either not significant or substantially low or negative.

Validity testing

The analysis will consider the following to determine the validity of the metric samples from the four processing methods: (1) If the metrics resulting from each processing method indicate high or low correlation overall; (2) If the landmark correlation values are similar for both the Paired Inter-Landmark (ILD) variation and the Landmark Point Variation (LPV) analysis; (3) If patterns in the correlation of the data be explained by the influence of factors within the sample; (4) If variations in correlation are due to random error that can be evaluated by examination of the coefficient of determination (covariance, R^2); and (5) Is systematic error present in the differences between the criterion direct digital landmark points and the landmark points of each process and confounding the findings of validity (Nance and Ball 1986; Carmines and Zeller 1979).

Camines and Zeller (1979) informs the levels of validity coefficients that are considered to reflect validity. For this study, the levels of correlation necessary are set to a moderate level - conservative to avoid validating data that is too variable to be really useful and moderate to account for the variability in terms of observation bias and individual cranial variations (size, sex, etc.) which represent variability in the resulting measurements under all landmark sample conditions. In cases of testing the validity of a new metric, the level of correlation need not be set at a highly conservative level. This reflects the instance that even moderate correlations suggest a probable improvement with the use of the new metric or method (Carmines and Zeller 1979).

The choice of criterion-related validity test also divides the collected samples for comparison between the Microscribe® (Revware, Raleigh, NC, USA) digitizer sample and the samples collected from the 3-D models. For a criterion-related test of validity, the rejection of validity is influenced by the presences of systematic error which does not necessarily reflect on the reliability of the test method.

Reliability is often tested concurrently with validity when this type of testing is undertaken. This is not applied to the current experimental design of this thesis. Justification for not applying reliability testing stems from the impact of multiple observers, and the testing of combinations of multiple process parameters. When multiple observers are involved in the collection of a sample of any time of observed metric, error and bias are increased and may not always be simple to pinpoint and account for in research design. For the research design of this thesis it was necessary to consider this and apply a test of validity that could inform the

results for trends that could be related to the differences in the measurements derived from the process models.

Repeating the data collection would have overcome the concerns created by the multiple original observers. However, for the purposes for testing multiple processing methods as applied here, it was not practical for a single observer to collect the landmarks samples from each of the four process models for each of the 13 crania in the sample more than once.

Chapter Four

Results

For nine crania of the sample, the non-manifold model is larger in size than the manifold counterpart. This suggests that some models contain components that were not removed at the higher face count during the processing steps. The observable results could be irregular face or vertex normals, or non-incident faces (Hoppe et al. 1993). The problems that could be caused in terms of the landmark selection process for the software and the observer using a mesh model with such defects are both real and subjective. The real problems arise when a point cannot connect with the observed surface at the coordinate it is being placed on. The subjective consequence for the observer it to either change the selection coordinate or note the point as missing for that landmark on the defective sample.

Table 5: Computational Characteristics of Processed Models

Model (*.PLY)			
Crania Code	*Proc Code*	*Crania*	*File size (MB)*
1	1	2go-2-2_m_hf.ply	2.9
1	2	2go-2-2_m_hfnm.ply	4.9
1	3	2go-2-2_m_lf.ply	1.0
1	4	2go-2-2_m_lfnm.ply	1.8
2	1	6go-6-6_m_hf.ply	2.9
2	2	6go-6-6_m_hfnm.ply	2.6
2	3	6go-6-6_m_lf.ply	1.0
2	4	6go-6-6_m_lfnm.ply	1.0
3	1	8-14_f_hf.ply	2.8
3	2	8-14_f_hfnm.ply	4.9
3	3	8-14_f_lf.ply	0.9
3	4	8-14_f_lfnm.ply	1.8
4	1	11-5_m_hf.ply	2.9
4	2	11-5_m_hfnm.ply	3.0
4	3	11-5_m_lf.ply	1.0
4	4	11-5_m_lfnm.ply	1.1
5	1	11-14_f_hf.ply	2.9
5	2	11-14_f_hfnm.ply	2.9
5	3	11-14_f_lf.ply	1.0
5	4	11-14_f_lfnm.ply	1.0
6	1	11-15_m_hf.ply	2.9
6	2	11-15_m_hfnm.ply	3.0
6	3	11-15_m_lf.ply	1.0
6	4	11-15_m_lfnm.ply	1.1
7	1	11-42_f_hf.ply	2.9
7	2	11-42_f_hfnm.ply	3.0
7	3	11-42_f_lf.ply	1.0
7	4	11-42_f_lfnm.ply	1.1

Model (*.PLY)			
Crania Code	*Proc Code*	*Crania*	*File size (MB)*
8	1	2go-2-30_m_hf.ply	2.9
8	2	2go-2-30_m_hfnm.ply	4.9
8	3	2go-2-30_m_lf.ply	1.0
8	4	2go-2-30_m_lfnm.ply	1.8
9	1	2go-2-32_m_hf.ply	2.9
9	2	2go-2-32_m_hfnm.ply	4.9
9	3	2go-2-32_m_lf.ply	1.0
9	4	2go-2-32_m_lfnm.ply	1.8
10	1	7-12_m_hf.ply	2.9
10	2	7-12_m_hfnm.ply	4.9
10	3	7-12_m_lf.ply	1.0
10	4	7-12_m_lfnm.ply	1.8
11	1	9-15_f_hf.ply	2.9
11	2	9-15_f_hfnm.ply	2.9
11	3	9-15_f_lf.ply	1.0
11	4	9-15_f_lfnm.ply	1.0
12	1	11-34_m_hf.ply	2.8
12	2	11-34_m_hfnm.ply	3.1
12	3	11-34_m_lf.ply	0.9
12	4	11-34_m_lfnm.ply	1.2
13	1	11-42_m_hf.ply	2.7
13	2	11-42_m_hfnm.ply	2.7
13	3	11-42_m_lf.ply	2.7
13	4	11-42_m_lfnm.ply	2.7
		Mean	2.3
		Min	0.9
		Max	4.9

Table 5 indicates a mean files size of 6.58 MB for one clean hemisphere. This would indicate a high likelihood a merged, unprocessed mesh could average greater than 13 MB. The size of a file becomes an issue for 3-D rendering as the file is dynamically read to reflect dimensions and movement in a semi-realistic digital environment.

This shows the file size reduction post processing for merged hemispheres for each processing parameter (HF, HFNM, LF, LFNM). Of note is the reduction in files size to a maximum files size that is less than the smallest files size for a single hemisphere of the raw models

Landmark Sample

During landmark selection, several non-manifold models for both processing resolutions were found to have defects that had a slight impact on the observation and selection of landmarks. For this sample, the defects were found to be non-incident faces that created defective geometry and caused the selected coordinate of a point to appear to exist below the surface to the crania. Wherever possible, selection coordinates for points were adjusted to reflect the observed surface of the cranial model.

Correlation analysis

Paired Inter-Landmark Distance

Correlation of the ILD with all unique paired landmarks characterizes the sensitivity of the measurements taken from the process models to the criterion distances from the Microscribe® (Revware, Raleigh, NC, USA) digitizer sample.

Table 6 lists the ILD by process and a summary for the correlation of each point. Tables 7-8 list ILD Correlations by landmark listing for all possible unique paired distances and the correlation coefficient.

There are landmarks with characteristics that result in a higher variability even when selected by the same observer in the same or different sessions. Such landmarks are classified by Bookstein (1997) as Type III. These landmarks have a very loosely bound definition and often are difficult to locate by definition using the Microscribe® (Revware, Raleigh, NC, USA) (Ross and Williams 2008; Sholts et al. 2011a). ANOVA GLM was applied with R software (Team 2014) and suggests the

relative distance differences from the paired ILD of the highlighted eight out of the 37 total sampled landmarks as having a higher relative variability.

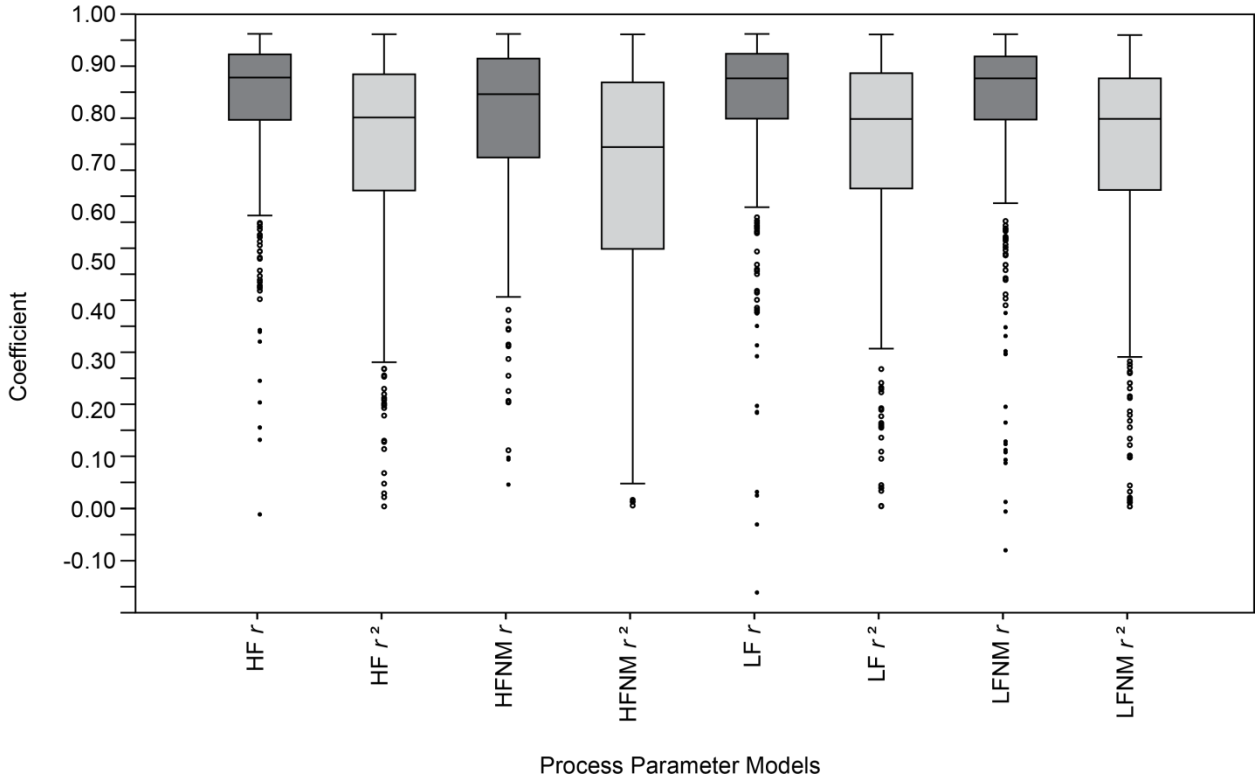

Figure 8: ILD Summary of Correlation (r) and COD (r^2) by Process

Correlation histograms are indicated by the darker filled regions. Three out of the four appear very similar, the correlation for the high face non-manifold differs being less constrained. The same pattern can be observed in the histograms of the covariance (lighter filled regions). This table summarizes the correlation and coefficient of determination tests of all ~666 non-repeating comparisons for each of the four sets of process parameters. Outliers are predominantly the result of and ILD with a Type III landmark point at one or both terminus of the distance.

Table 6: Summary of Inter-Landmark Distance Correlation by Process

Correlation Distribution						
For All Points						
Process	*Mean*	*Std Error*	*Std Deviation*	*s Variance*	*Max*	*Min*
hf	0.8607	0.0057	0.1478	0.0218	0.9992	-0.0166
hfnm	0.8356	0.0064	0.1654	0.0274	0.9991	0.0464
lf	0.8681	0.0059	0.1524	0.0232	0.9980	-0.1818
lfnm	0.8602	0.0066	0.1690	0.0286	0.9987	-0.1833

Table 7: ILD Correlation by Point (hf & hfnm)

	Correlation Coefficient (Pearson's r / Spearman's rs)											
	Type	**Point**	***Process***	***Coef.***	***COD***	***Min***	***Max***	***Process***	***Coef.***	***COD***	***Min***	***Max***
1	**2**	**prosH**	hf	**0.8671**	0.7519	0.3960	0.9874	hfnm	**0.8310**	0.6906	0.3031	0.9848
2	**2**	**ssp**	hf	**0.8950**	0.8010	0.3486	0.9924	hfnm	0.7728	0.5972	0.4432	0.9655
3	**2**	**prosM**	hf	**0.8003**	0.6405	0.3960	0.9474	hfnm	0.7210	0.5198	0.2765	0.9202
4	**1**	**nas**	hf	**0.8564**	0.7334	-0.0166	0.9944	hfnm	**0.8496**	0.7218	0.3120	0.9940
5	**3**	**glb**	hf	**0.8242**	0.6793	0.1671	0.9917	hfnm	0.7974	0.6358	0.2234	0.9917
6	**3**	**spglb**	hf	0.6467	0.4182	0.1671	0.9803	hfnm	0.7936	0.6298	0.0464	0.9752
7	**1**	**brg**	hf	**0.8969**	0.8044	0.2201	0.9883	hfnm	**0.8673**	0.7522	0.0464	0.9876
8	**1**	**lam**	hf	**0.9099**	0.8279	0.3731	0.9946	hfnm	**0.8715**	0.7595	0.2290	0.9961
9	**3**	**opg**	hf	**0.8948**	0.8007	0.3731	0.9965	hfnm	**0.8640**	0.7465	0.3425	0.9987
10	**2**	**ops**	hf	**0.9100**	0.8281	0.2757	0.9917	hfnm	**0.8866**	0.7861	0.4160	0.9940
11	**2**	**bas**	hf	**0.8710**	0.7586	0.4564	0.9806	hfnm	**0.8653**	0.7487	0.5661	0.9939
12	**3**	**zygomr**	hf	**0.8906**	0.7932	0.2782	0.9874	hfnm	**0.8485**	0.7200	0.3923	0.9825
13	**2**	**jugr**	hf	**0.8659**	0.7498	0.2467	0.9967	hfnm	**0.8689**	0.7550	0.3923	0.9981
14	**3**	**fmtr**	hf	**0.8565**	0.7336	0.4398	0.9733	hfnm	**0.8630**	0.7448	0.3847	0.9908
15	**3**	**fmar**	hf	**0.9079**	0.8243	0.5975	0.9840	hfnm	**0.9049**	0.8188	0.1311	0.9914
16	**3**	**ectr**	hf	**0.8774**	0.7698	0.6071	0.9839	hfnm	**0.8864**	0.7857	0.5380	0.9821
17	**2**	**zygoor**	hf	0.7965	0.6344	0.3944	0.9777	hfnm	**0.8182**	0.6695	0.3878	0.9908
18	**2**	**dacr**	hf	**0.8580**	0.7362	0.4914	0.9942	hfnm	**0.8003**	0.6405	0.0995	0.9988
19	**2**	**dacl**	hf	**0.8410**	0.7073	0.2467	0.9934	hfnm	**0.8386**	0.7032	0.4994	0.9936
20	**3**	**obhi**	hf	**0.8682**	0.7538	0.4622	0.9976	hfnm	**0.8503**	0.7230	0.5300	0.9988
21	**3**	**obhs**	hf	**0.8114**	0.6584	-0.0166	0.9918	hfnm	**0.8021**	0.6434	0.2234	0.9967
22	**3**	**ectl**	hf	**0.8992**	0.8086	0.5252	0.9976	hfnm	**0.8997**	0.8095	0.5387	0.9988
23	**2**	**zygool**	hf	**0.8617**	0.7425	0.5524	0.9796	hfnm	0.7152	0.5115	0.1190	0.9904
24	**3**	**fmal**	hf	**0.8608**	0.7410	0.4648	0.9836	hfnm	**0.8411**	0.7074	0.1190	0.9914
25	**3**	**fmtl**	hf	**0.8658**	0.7496	0.5914	0.9699	hfnm	**0.8072**	0.6516	0.3738	0.9932
26	**2**	**jugl**	hf	**0.8705**	0.7578	0.1410	0.9731	hfnm	**0.8493**	0.7213	0.2202	0.9922
27	**3**	**zygoml**	hf	**0.8643**	0.7470	0.3486	0.9897	hfnm	**0.8301**	0.6891	0.1033	0.9925
28	**3**	**zygl**	hf	**0.8070**	0.6512	0.3944	0.9936	hfnm	0.7618	0.5803	0.2202	0.9970
29	**3**	**zygr**	hf	**0.8200**	0.6724	0.1410	0.9902	hfnm	**0.8124**	0.6600	0.1033	0.9962
30	**3**	**eurr**	hf	**0.8461**	0.7159	0.5252	0.9922	hfnm	**0.8074**	0.6519	0.4705	0.9970
31	**3**	**eurl**	hf	**0.8587**	0.7374	0.4971	0.9951	hfnm	**0.8023**	0.6437	0.0995	0.9821
32	**1**	**stpl**	hf	**0.8481**	0.7193	0.4670	0.9946	hfnm	**0.8470**	0.7174	0.5028	0.9961
33	**1**	**stpr**	hf	**0.8361**	0.6991	0.2658	0.9967	hfnm	**0.8362**	0.6992	0.5085	0.9987
34	**3**	**porr**	hf	**0.9047**	0.8185	0.2782	0.9992	hfnm	**0.8357**	0.6984	0.1311	0.9991
35	**3**	**porl**	hf	**0.9169**	0.8407	0.4734	0.9967	hfnm	**0.8705**	0.7578	0.3847	0.9981
36	**2**	**mastr**	hf	**0.9236**	0.8530	0.7186	0.9992	hfnm	**0.9035**	0.8163	0.6078	0.9991
37	**2**	**mastl**	hf	**0.9173**	0.8414	0.6731	0.9967	hfnm	**0.8966**	0.8039	0.5984	0.9945

Highlight indicates points with lowest correlations across all process methods.

Table 8: ILD Correlation by Point (lf & lfnm)

	Correlation Coefficient (Pearson's r / Spearman's rs) (cont.)										
	Type	**Point**	***Process***	***Coef.***	***COD***	***Min***	***Max***	***Process***	***Coef.***	***COD***	***Min***	***Max***
1	**2**	**prosH**	lf	**0.8767**	0.7686	0.2203	0.9903	lfnm	**0.8806**	0.7755	0.4688	0.9853
2	**2**	**ssp**	lf	**0.8792**	0.7730	0.5930	0.9927	lfnm	**0.8853**	0.7838	0.5823	0.9868
3	**2**	**prosM**	lf	0.7954	0.6327	0.2203	0.9544	lfnm	0.7998	0.6397	0.4688	0.9694
4	**1**	**nas**	lf	**0.8598**	0.7393	-0.0379	0.9930	lfnm	**0.8562**	0.7331	0.0920	0.9875
5	**3**	**glb**	lf	0.7994	0.6390	0.1981	0.9942	lfnm	**0.8039**	0.6463	0.1195	0.9895
6	**3**	**spglb**	lf	0.7640	0.5837	-0.1818	0.9790	lfnm	0.6284	0.3949	-0.0105	0.9775
7	**1**	**brg**	lf	**0.8483**	0.7196	-0.1818	0.9891	lfnm	**0.9036**	0.8165	-0.0105	0.9828
8	**1**	**lam**	lf	**0.9155**	0.8381	0.4108	0.9940	lfnm	**0.8989**	0.8080	0.0987	0.9962
9	**3**	**opg**	lf	**0.8998**	0.8096	0.4108	0.9983	lfnm	**0.9005**	0.8109	0.0987	0.9987
10	**2**	**ops**	lf	**0.9295**	0.8640	0.5601	0.9955	lfnm	**0.9334**	0.8712	0.7245	0.9924
11	**2**	**bas**	lf	**0.8994**	0.8089	0.5008	0.9946	lfnm	**0.8855**	0.7841	0.6501	0.9910
12	**3**	**zygomr**	lf	**0.8894**	0.7910	0.3960	0.9885	lfnm	**0.8685**	0.7543	0.4285	0.9828
13	**2**	**jugr**	lf	**0.8986**	0.8075	0.5028	0.9981	lfnm	**0.8915**	0.7948	0.1955	0.9969
14	**3**	**fmtr**	lf	**0.8829**	0.7795	0.6037	0.9931	lfnm	**0.8802**	0.7748	0.5357	0.9839
15	**3**	**fmar**	lf	**0.9319**	0.8684	0.7628	0.9923	lfnm	**0.9177**	0.8422	0.3222	0.9833
16	**3**	**ectr**	lf	**0.8862**	0.7854	0.5965	0.9895	lfnm	**0.8789**	0.7725	0.4764	0.9847
17	**2**	**zygoor**	lf	**0.8213**	0.6745	0.3455	0.9855	lfnm	**0.8076**	0.6522	-0.1833	0.9876
18	**2**	**dacr**	lf	**0.8800**	0.7744	0.6586	0.9966	lfnm	**0.8731**	0.7623	0.5310	0.9976
19	**2**	**dacl**	lf	**0.8570**	0.7344	0.5028	0.9927	lfnm	**0.8709**	0.7585	0.3228	0.9924
20	**3**	**obhi**	lf	**0.8945**	0.8001	0.4082	0.9962	lfnm	**0.8826**	0.7790	0.4398	0.9959
21	**3**	**obhs**	lf	**0.8377**	0.7017	-0.0379	0.9938	lfnm	**0.8176**	0.6685	0.0097	0.9941
22	**3**	**ectl**	lf	**0.8965**	0.8037	0.4370	0.9966	lfnm	**0.9062**	0.8212	0.4092	0.9976
23	**2**	**zygool**	lf	**0.8240**	0.6790	0.2128	0.9927	lfnm	**0.8199**	0.6722	0.1776	0.9849
24	**3**	**fmal**	lf	**0.8693**	0.7557	0.1999	0.9860	lfnm	**0.8637**	0.7460	0.5108	0.9822
25	**3**	**fmtl**	lf	**0.8424**	0.7096	0.4521	0.9802	lfnm	0.7993	0.6389	0.1148	0.9872
26	**2**	**jugl**	lf	**0.8557**	0.7322	0.0309	0.9831	lfnm	**0.8728**	0.7618	0.1322	0.9875
27	**3**	**zygoml**	lf	**0.8451**	0.7142	0.0234	0.9923	lfnm	**0.8289**	0.6871	-0.0925	0.9908
28	**3**	**zygl**	lf	0.7954	0.6327	0.0309	0.9969	lfnm	0.7783	0.6058	-0.1833	0.9940
29	**3**	**zygr**	lf	**0.8301**	0.6891	0.0234	0.9943	lfnm	**0.8174**	0.6681	-0.0925	0.9908
30	**3**	**eurr**	lf	**0.8411**	0.7074	0.1999	0.9973	lfnm	**0.8406**	0.7066	0.4092	0.9923
31	**3**	**eurl**	lf	**0.8711**	0.7588	0.3178	0.9916	lfnm	**0.8646**	0.7475	0.3284	0.9815
32	**1**	**stpl**	lf	**0.8629**	0.7446	0.5561	0.9981	lfnm	**0.8772**	0.7695	0.5481	0.9962
33	**1**	**stpr**	lf	**0.8691**	0.7553	0.5114	0.9983	lfnm	**0.8318**	0.6919	0.2109	0.9987
34	**3**	**porr**	lf	**0.9036**	0.8165	0.3960	0.9990	lfnm	**0.9039**	0.8170	0.4285	0.9984
35	**3**	**porl**	lf	**0.9162**	0.8394	0.4906	0.9979	lfnm	**0.9190**	0.8446	0.6173	0.9969
36	**2**	**mastr**	lf	**0.9245**	0.8547	0.6586	0.9990	lfnm	**0.9241**	0.8540	0.5854	0.9984
37	**2**	**mastl**	lf	**0.9269**	0.8591	0.6992	0.9962	lfnm	**0.9136**	0.8347	0.6485	0.9969
Highlight indicates points with lowest correlations across all process methods.												

Table 9: ILD ANOVA GLM (High Face Count, Manifold)

			HF				F-statistic:			
	Point	Type	Mtpl R^2:	R:	Adj R^2:	R:		DF	DF	p-value:
1	***prosH***	2	0.8144	0.9024	0.8140	0.9022	2050	2	934	<2.2e-16
2	ssp	2	0.7927	0.8903	0.7922	0.8901	1786	2	934	<2.2e-16
3	prosM	2	0.8094	0.8997	0.8090	0.8994	1983	2	934	<2.2e-16
4	nas	1	0.7773	0.8816	0.7768	0.8814	1630	2	934	<2.2e-16
5	glb	3	0.7987	0.8937	0.7983	0.8935	1853	2	934	<2.2e-16
6	spglb	3	0.8339	0.9132	0.8336	0.9130	2345	2	934	<2.2e-16
7	brg	1	0.9661	0.9829	0.9660	0.9829	1.33E+04	2	934	<2.2e-16
8	lam	1	0.9480	0.9737	0.9479	0.9736	8516	2	934	<2.2e-16
9	opg	3	0.9451	0.9722	0.9450	0.9721	8046	2	934	<2.2e-16
10	***ops***	2	0.9500	0.9747	0.9499	0.9746	8880	2	934	<2.2e-16
11	***bas***	2	0.9548	0.9771	0.9547	0.9771	9870	2	934	<2.2e-16
12	zygomr	3	0.8354	0.9140	0.8350	0.9138	2370	2	934	<2.2e-16
13	***jugr***	2	0.8373	0.9150	0.8370	0.9149	2404	2	934	<2.2e-16
14	fmtr	3	0.8319	0.9121	0.8316	0.9119	2311	2	934	<2.2e-16
15	fmar	3	0.8198	0.9054	0.8194	0.9052	2125	2	934	<2.2e-16
16	ectr	3	0.8118	0.9010	0.8114	0.9008	2015	2	934	<2.2e-16
17	zygoor	2	0.7948	0.8915	0.7944	0.8913	1809	2	934	<2.2e-16
18	dacr	2	0.7893	0.8884	0.7888	0.8881	1749	2	934	<2.2e-16
19	dacl	2	0.7731	0.8793	0.7727	0.8790	1592	2	934	<2.2e-16
20	obhi	3	0.7666	0.8756	0.7661	0.8753	1534	2	934	<2.2e-16
21	obhs	3	0.7935	0.8908	0.793	0.8905	1794	2	934	<2.2e-16
22	ectl	3	0.7811	0.8838	0.7806	0.8835	1666	2	934	<2.2e-16
23	zygool	2	0.7632	0.8736	0.7627	0.8733	1506	2	934	<2.2e-16
24	fmal	3	0.7888	0.8881	0.7884	0.8879	1744	2	934	<2.2e-16
25	fmtl	3	0.8050	0.8972	0.8046	0.8970	1928	2	934	<2.2e-16
26	jugl	2	0.8131	0.9017	0.8127	0.9015	2032	2	934	<2.2e-16
27	zygoml	3	0.8126	0.9014	0.8122	0.9012	2025	2	934	<2.2e-16
28	***zygl***	3	0.8685	0.9319	0.8682	0.9318	3085	2	934	<2.2e-16
29	***zygr***	3	0.8788	0.9374	0.8785	0.9373	3385	2	934	<2.2e-16
30	eurr	3	0.9397	0.9694	0.9395	0.9693	7273	2	934	<2.2e-16
31	eurl	3	0.9408	0.9699	0.9406	0.9698	7417	2	934	<2.2e-16
32	stpl	1	0.9297	0.9642	0.9295	0.9641	6172	2	934	<2.2e-16
33	stpr	1	0.9340	0.9664	0.9338	0.9663	6604	2	934	<2.2e-16
34	porr	3	0.9180	0.9581	0.9179	0.9581	5230	2	934	<2.2e-16
35	porl	3	0.9171	0.9577	0.9169	0.9575	5167	2	934	<2.2e-16
36	***mastr***	2	0.9318	0.9653	0.9317	0.9652	6381	2	934	<2.2e-16
37	***mastl***	2	0.9337	0.9663	0.9335	0.9662	6575	2	934	<2.2e-16

Bold landmark names indicate landmarks with missing values.
Highlight indicates points with higher variation.

Table 10: ILD ANOVA GLM (High Face Count, Non-manifold)

			HFNM				F-statistic:			
	Point	Type	Mtpl R^2	R:	Adj R^2:	R:		DF	DF	p-value:
1	***prosH***	2	0.8141	0.9023	0.8137	0.9021	2046	2	934	<2.2e-16
2	ssp	2	0.7942	0.8912	0.7938	0.8910	1802	2	934	<2.2e-16
3	prosM	2	0.8097	0.8998	0.8093	0.8996	1987	2	934	<2.2e-16
4	nas	1	0.7768	0.8814	0.7763	0.8811	1625	2	934	<2.2e-16
5	glb	3	0.7973	0.8929	0.7969	0.8927	1837	2	934	<2.2e-16
6	spglb	3	0.8319	0.9121	0.8315	0.9119	2311	2	934	<2.2e-16
7	brg	1	0.9664	0.9831	0.9663	0.9830	1.34E+04	2	934	<2.2e-16
8	lam	1	0.9479	0.9736	0.9478	0.9736	8504	2	934	<2.2e-16
9	opg	3	0.9451	0.9722	0.9450	0.9721	8040	2	934	<2.2e-16
10	***ops***	2	0.9502	0.9748	0.9501	0.9747	8911	2	934	<2.2e-16
11	***bas***	2	0.9556	0.9775	0.9555	0.9775	1.01E+04	2	934	<2.2e-16
12	zygomr	3	0.8355	0.9141	0.8351	0.9138	2371	2	934	<2.2e-16
13	***jugr***	2	0.8363	0.9145	0.8360	0.9143	2386	2	934	<2.2e-16
14	fmtr	3	0.8316	0.9119	0.8312	0.9117	2306	2	934	<2.2e-16
15	fmar	3	0.8197	0.9054	0.8193	0.9052	2123	2	934	<2.2e-16
16	ectr	3	0.8114	0.9008	0.8110	0.9006	2009	2	934	<2.2e-16
17	zygoor	2	0.7947	0.8915	0.7942	0.8912	1807	2	934	<2.2e-16
18	dacr	2	0.7898	0.8887	0.7893	0.8884	1755	2	934	<2.2e-16
19	dacl	2	0.7721	0.8787	0.7716	0.8784	1582	2	934	<2.2e-16
20	obhi	3	0.7668	0.8757	0.7663	0.8754	1535	2	934	<2.2e-16
21	obhs	3	0.7928	0.8904	0.7924	0.8902	1787	2	934	<2.2e-16
22	ectl	3	0.7812	0.8839	0.7807	0.8836	1667	2	934	<2.2e-16
23	zygool	2	0.7636	0.8738	0.7631	0.8736	1509	2	934	<2.2e-16
24	fmal	3	0.7886	0.8880	0.7881	0.8877	1742	2	934	<2.2e-16
25	fmtl	3	0.8053	0.8974	0.8049	0.8972	1932	2	934	<2.2e-16
26	jugl	2	0.8143	0.9024	0.8139	0.9022	2048	2	934	<2.2e-16
27	zygoml	3	0.8133	0.9018	0.8129	0.9016	2035	2	934	<2.2e-16
28	***zygl***	3	0.8679	0.9316	0.8676	0.9315	3067	2	934	<2.2e-16
29	***zygr***	3	0.8775	0.9367	0.8772	0.9366	3344	2	934	<2.2e-16
30	eurr	3	0.9402	0.9696	0.9401	0.9696	7344	2	934	<2.2e-16
31	eurl	3	0.9408	0.9699	0.9407	0.9699	7419	2	934	<2.2e-16
32	stpl	1	0.9281	0.9634	0.9279	0.9633	6025	2	934	<2.2e-16
33	stpr	1	0.9331	0.9660	0.9330	0.9659	6514	2	934	<2.2e-16
34	porr	3	0.9183	0.9583	0.9182	0.9582	5251	2	934	<2.2e-16
35	porl	3	0.9176	0.9579	0.9175	0.9579	5203	2	934	<2.2e-16
36	***mastr***	2	0.9323	0.9656	0.9322	0.9655	6432	2	934	<2.2e-16
37	***mastl***	2	0.9343	0.9666	0.9342	0.9665	6643	2	934	<2.2e-16

Bold landmark names indicate landmarks with missing values.
Highlight indicates points with higher variation.

Table 11: ILD ANOVA GLM (Low Face Count, Manifold)

			LF				F-statistic:			
	Point	Type	Mtpl R^2	R:	Adj R^2:	R:		DF	DF	p-value:
1	***prosH***	2	0.8142	0.9023	0.8138	0.9021	2046	2	934	<2.2e-16
2	ssp	2	0.7924	0.8902	0.7920	0.8899	1783	2	934	<2.2e-16
3	prosM	2	0.8092	0.8996	0.8088	0.8993	1981	2	934	<2.2e-16
4	nas	1	0.7769	0.8814	0.7764	0.8811	1626	2	934	<2.2e-16
5	glb	3	0.7985	0.8936	0.7980	0.8933	1850	2	934	<2.2e-16
6	spglb	3	0.8331	0.9127	0.8328	0.9126	2331	2	934	<2.2e-16
7	brg	1	0.9662	0.9830	0.9661	0.9829	1.34E+04	2	934	<2.2e-16
8	lam	1	0.9478	0.9736	0.9477	0.9735	8486	2	934	<2.2e-16
9	opg	3	0.9451	0.9722	0.9450	0.9721	8045	2	934	<2.2e-16
10	***ops***	2	0.9502	0.9748	0.9501	0.9747	8915	2	934	<2.2e-16
11	***bas***	2	0.9550	0.9772	0.9549	0.9772	9917	2	934	<2.2e-16
12	zygomr	3	0.8347	0.9136	0.8344	0.9135	2359	2	934	<2.2e-16
13	***jugr***	2	0.8367	0.9147	0.8363	0.9145	2392	2	934	<2.2e-16
14	fmtr	3	0.8319	0.9121	0.8316	0.9119	2312	2	934	<2.2e-16
15	fmar	3	0.8199	0.9055	0.8195	0.9053	2126	2	934	<2.2e-16
16	ectr	3	0.8114	0.9008	0.8110	0.9006	2009	2	934	<2.2e-16
17	zygoor	2	0.7943	0.8912	0.7938	0.8910	1803	2	934	<2.2e-16
18	dacr	2	0.7886	0.8880	0.7881	0.8877	1742	2	934	<2.2e-16
19	dacl	2	0.7726	0.8790	0.7721	0.8787	1587	2	934	<2.2e-16
20	obhi	3	0.7666	0.8756	0.7661	0.8753	1534	2	934	<2.2e-16
21	obhs	3	0.7933	0.8907	0.7929	0.8904	1792	2	934	<2.2e-16
22	ectl	3	0.7812	0.8839	0.7807	0.8836	1667	2	934	<2.2e-16
23	zygool	2	0.7634	0.8737	0.7629	0.8734	1507	2	934	<2.2e-16
24	fmal	3	0.7890	0.8883	0.7886	0.8880	1747	2	934	<2.2e-16
25	fmtl	3	0.8051	0.8973	0.8047	0.8971	1929	2	934	<2.2e-16
26	jugl	2	0.8135	0.9019	0.8131	0.9017	2037	2	934	<2.2e-16
27	zygoml	3	0.8126	0.9014	0.8122	0.9012	2025	2	934	<2.2e-16
28	***zygl***	3	0.8684	0.9319	0.8681	0.9317	3081	2	934	<2.2e-16
29	***zygr***	3	0.8784	0.9372	0.8781	0.9371	3374	2	934	<2.2e-16
30	eurr	3	0.9403	0.9697	0.9402	0.9696	7354	2	934	<2.2e-16
31	eurl	3	0.9413	0.9702	0.9411	0.9701	7485	2	934	<2.2e-16
32	stpl	1	0.9290	0.9638	0.9289	0.9638	6113	2	934	<2.2e-16
33	stpr	1	0.9337	0.9663	0.9336	0.9662	6581	2	934	<2.2e-16
34	porr	3	0.9186	0.9584	0.9184	0.9583	5271	2	934	<2.2e-16
35	porl	3	0.9174	0.9578	0.9172	0.9577	5184	2	934	<2.2e-16
36	***mastr***	2	0.9323	0.9656	0.9321	0.9655	6428	2	934	<2.2e-16
37	***mastl***	2	0.9338	0.9663	0.9337	0.9663	6592	2	934	<2.2e-16

Bold landmark names indicate landmarks with missing values.
Highlight indicates points with higher variation.

Table 12: ILD ANOVA GLM (Low Face Count, Non-manifold)

			LFNM				F-statistic:			
	Point	Type	Mtpl R^2	R:	Adj R^2:	R:		DF	DF	p-value:
1	***prosH***	2	0.8137	0.9021	0.8133	0.9018	2040	2	934	<2.2e-16
2	ssp	2	0.7933	0.8907	0.7928	0.8904	1792	2	934	<2.2e-16
3	prosM	2	0.8091	0.8995	0.8087	0.8993	1979	2	934	<2.2e-16
4	nas	1	0.7773	0.8816	0.7768	0.8814	1630	2	934	<2.2e-16
5	glb	3	0.7991	0.8939	0.7986	0.8936	1857	2	934	<2.2e-16
6	spglb	3	0.8332	0.9128	0.8328	0.9126	2332	2	934	<2.2e-16
7	brg	1	0.9658	0.9828	0.9658	0.9828	1.32E+04	2	934	<2.2e-16
8	lam	1	0.9477	0.9735	0.9476	0.9734	8469	2	934	<2.2e-16
9	opg	3	0.9450	0.9721	0.9449	0.9721	8029	2	934	<2.2e-16
10	***ops***	2	0.9502	0.9748	0.9501	0.9747	8905	2	934	<2.2e-16
11	***bas***	2	0.9554	0.9774	0.9553	0.9774	1.00E+04	2	934	<2.2e-16
12	zygomr	3	0.8353	0.9139	0.8350	0.9138	2369	2	934	<2.2e-16
13	***jugr***	2	0.8370	0.9149	0.8366	0.9147	2398	2	934	<2.2e-16
14	fmtr	3	0.8323	0.9123	0.8319	0.9121	2317	2	934	<2.2e-16
15	fmar	3	0.8201	0.9056	0.8198	0.9054	2130	2	934	<2.2e-16
16	ectr	3	0.8117	0.9009	0.8113	0.9007	2013	2	934	<2.2e-16
17	zygoor	2	0.7949	0.8916	0.7945	0.8913	1810	2	934	<2.2e-16
18	dacr	2	0.7886	0.8880	0.7881	0.8877	1742	2	934	<2.2e-16
19	dacl	2	0.7725	0.8789	0.7720	0.8786	1585	2	934	<2.2e-16
20	obhi	3	0.7665	0.8755	0.7660	0.8752	1533	2	934	<2.2e-16
21	obhs	3	0.7945	0.8913	0.7941	0.8911	1806	2	934	<2.2e-16
22	ectl	3	0.7807	0.8836	0.7803	0.8833	1663	2	934	<2.2e-16
23	zygool	2	0.7634	0.8737	0.7629	0.8734	1507	2	934	<2.2e-16
24	fmal	3	0.7885	0.8880	0.7880	0.8877	1741	2	934	<2.2e-16
25	fmtl	3	0.8051	0.8973	0.8047	0.8971	1930	2	934	<2.2e-16
26	jugl	2	0.8134	0.9019	0.8130	0.9017	2036	2	934	<2.2e-16
27	zygoml	3	0.8130	0.9017	0.8126	0.9014	2031	2	934	<2.2e-16
28	***zygl***	3	0.8670	0.9311	0.8667	0.9310	3044	2	934	<2.2e-16
29	***zygr***	3	0.8786	0.9373	0.8783	0.9372	3378	2	934	<2.2e-16
30	eurr	3	0.9404	0.9697	0.9402	0.9696	7365	2	934	<2.2e-16
31	eurl	3	0.9411	0.9701	0.9410	0.9701	7463	2	934	<2.2e-16
32	stpl	1	0.9289	0.9638	0.9287	0.9637	6100	2	934	<2.2e-16
33	stpr	1	0.9338	0.9663	0.9336	0.9662	6586	2	934	<2.2e-16
34	porr	3	0.9185	0.9584	0.9183	0.9583	5261	2	934	<2.2e-16
35	porl	3	0.9176	0.9579	0.9174	0.9578	5197	2	934	<2.2e-16
36	***mastr***	2	0.9325	0.9657	0.9323	0.9656	6450	2	934	<2.2e-16
37	***mastl***	2	0.9344	0.9666	0.9342	0.9665	6649	2	934	<2.2e-16

Bold landmark names indicate landmarks with missing values.
Highlight indicates points with higher variation.

Landmark Point Variation

Considering the plot of the LPV distribution, several effects of expected random error can be observed at this stage. Differentiating the landmarks based on type, groupings emerge. Clusters of Type I landmark points are expected given the constrained definition of Type I landmarks. Type II landmarks are vertically clustered on the plot, this is the result of greater distances to the Microscribe® (Revware, Raleigh, NC, USA) digitizer points than between the point coordinates of the process models.

The outliers on the plot of the distribution of the LPV sample differences are porion left and right, and supraglabellare. The porion landmarks are expected to be outliers because they are used in the application of the alignment procedure to the Frankfurt Horizontal. The reason for supraglabellare to be an outlier is likely due to definition and selection difference between observers. However, for these reasons, as well as the relatively high variation of several other Type III Landmarks, they are excluded from the LPV Mantel tests.

As a group, the Type I landmarks tested in the LPV sample have sufficient correlation and significance to conclude the validity for all process parameters for the selection of landmark points. For the high-face manifold subsample, all tests are significant as having a p-value of less than 0.005, the correlation range is 0.5691-0.9470, and the COD (R^2) range is 0.3239-0.8968. This indicates that for the landmark point with the lowest COD, approximately 32% of the variation can be attributed to the model, but 68% may be attributed to confounding or unknown variability. The results for the low-face non-manifold process are very similar to the

high-face manifold for correlation (0.6933-0.9093) and COD (0.4807-0.8268), having the same landmark points indicating lower correlations and lower COD values. The high-face non-manifold and low-face manifold processes both only have a single landmark point with a COD less than 0.5, and those points are different. The high-face non-manifold result for correlation range is 0.6873-0.9425, and the range for this process COD is 0.4724-0.8883. The low-face non-manifold result for correlation range is 0.5671-0.8820, and the range for COD is 0.3216-0.7779. Both non-manifold processes have a reduced maximum correlation and COD than the manifold process for the resolution group to which they belong.

Table 13: Landmark Point Variation Mantel Test by Point by Process

		R	p-value	R^2	R	p-value	R^3	R	p-value	R^4	R	p-value	R^5
Point	Type	HF	HF	HF	HFNM	HFNM	HFNM	LF	LF	LF	LFNM	LFNM	LFNM
nas	1	0.9470	0.0001	0.8968	0.9425	0.0001	0.8883	0.9093	0.0001	0.8268	0.8659	0.0001	0.7498
brg	1	0.7965	0.0001	0.6344	0.6873	0.0003	0.4724	0.7853	0.0001	0.6167	0.8820	0.0001	0.7779
lam	1	0.6582	0.0001	0.4332	0.8020	0.0001	0.6432	0.6933	0.0001	0.4807	0.5671	0.0001	0.3216
stpl	1	0.5975	0.0010	0.3570	0.7581	0.0001	0.5747	0.7383	0.0001	0.5451	0.6861	0.0001	0.4707
stpr	1	0.5691	0.0002	0.3239	0.7787	0.0001	0.6064	0.8157	0.0001	0.6654	0.6221	0.0001	0.3870
prosH	2	0.9186	0.0001	0.8438	0.8016	0.0001	0.6426	0.8947	0.0001	0.8005	0.8800	0.0001	0.7744
ssp	2	0.9106	0.0001	0.8292	0.2418	*0.0469*	0.0585	0.9155	0.0001	0.8381	0.9095	0.0001	0.8272
prosM	2	0.9279	0.0001	0.8610	0.8492	0.0001	0.7211	0.9144	0.0001	0.8361	0.8778	0.0001	0.7705
ops	2	0.8007	0.0001	0.6411	0.8837	0.0001	0.7809	0.8372	0.0001	0.7009	0.8732	0.0001	0.7625
bas	2	0.6453	0.0005	0.4164	0.6344	0.0004	0.4025	0.6645	0.0001	0.4416	0.6516	0.0001	0.4246
jugr	2	0.4564	0.0045	0.2083	0.7359	0.0001	0.5415	0.7188	0.0001	0.5167	0.5428	0.0003	0.2946
zygoor	2	0.8266	0.0001	0.6833	0.8859	0.0001	0.7848	0.8808	0.0001	0.7758	0.8913	0.0001	0.7944
dacr	2	0.8820	0.0001	0.7779	0.3944	0.0007	0.1556	0.7895	0.0001	0.6233	0.7762	0.0001	0.6025
dacl	2	0.8794	0.0001	0.7733	0.7954	0.0001	0.6327	0.7773	0.0001	0.6042	0.7538	0.0001	0.5682
zygool	2	0.8816	0.0001	0.7772	0.7472	0.0001	0.5583	0.8441	0.0001	0.7125	0.8910	0.0001	0.7939
jugl	2	0.8754	0.0001	0.7663	0.8324	0.0001	0.6929	0.8857	0.0001	0.7845	0.8847	0.0001	0.7827
mastr	2	0.9439	0.0001	0.8909	0.9520	0.0001	0.9063	0.9363	0.0001	0.8767	0.9407	0.0001	0.8849
mastl	2	0.9718	0.0001	0.9444	0.9497	0.0001	0.9019	0.9363	0.0001	0.8767	0.9055	0.0001	0.8199

Highlighting indicates an R^2 value below 0.5. *Italics indicate a p-value greater than .005.*

Table 14: Summary of Range of LVP Mantel Test by Type by Process

		HF		HFNM		LF		LFNM	
		R	R^2	R	R^3	R	R^4	R	R^5
Type 1	max	0.9470	0.8968	0.9425	0.8883	0.9093	0.8268	0.8820	0.7779
	min	0.5691	0.3239	0.6873	0.4724	0.6933	0.4807	0.5671	0.3216
Type 2	max	0.9718	0.9444	0.9520	0.9063	0.9363	0.8767	0.9407	0.8849
	min	0.4564	0.2083	0.2418	0.0585	0.6645	0.4416	0.5428	0.2946
All	avg	0.8049	0.6699	0.6699	0.0028	0.0028	0.8298	0.8298	0.6957

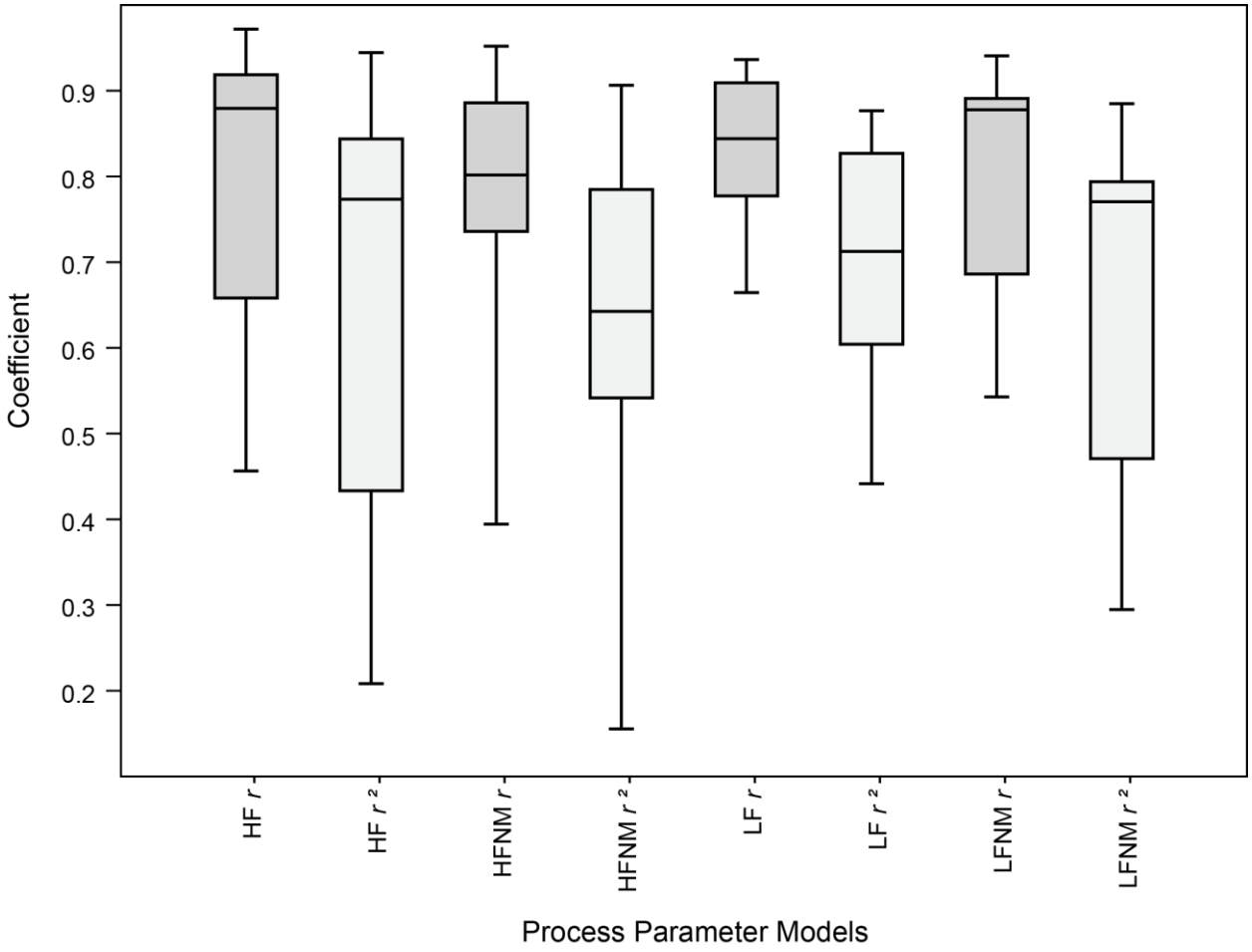

Figure 9: LPV Mantel Correlation (r) and COD (r^2) by Process

Correlation histograms are indicated by the darker filled regions. These histograms indicate wide variation and a tendency of positive skew. The correlation for the low face manifold landmark points has the last spread and skew, as well as the most overall constraint. A similar, but less constrained pattern can be observed in the histograms of the covariance (lighter filled regions).

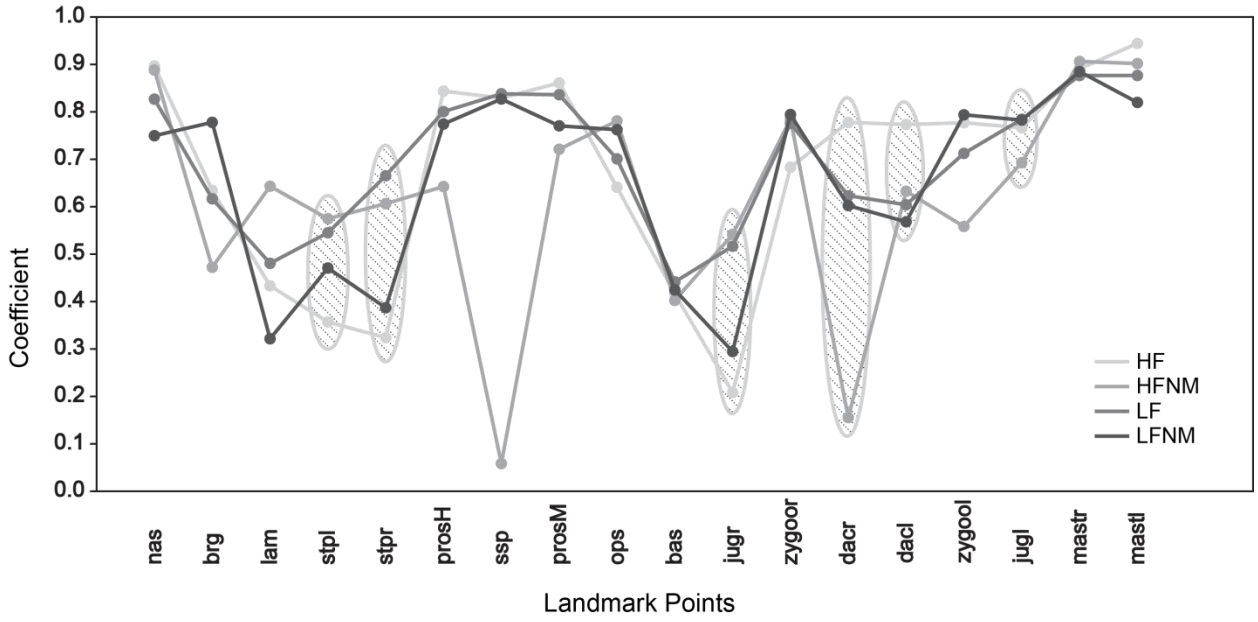

Figure 10: Plot of LPV Mantel COD (r^2) by Point for All Processes
Circled areas indicate lateral paired landmarks with more highly constrained correlation for the left point than the right point (stephanion (l, r), jugale (l, r), and dacryon (l, r)). The exception in this plot is the mastoideale lateral paired landmark points.

Attempting to determine the presence or likelihood of systematic error in the landmark point selection for each type of process model is to determine whether a process model landmark points have a consistent bias from the criterion method. Figure 10 is a plot of the Coefficient of Determination for the Type I and II points for all models for the LPV sample. The interaction of the lines across the plot indicates the lack of a systematic error or bias by either the Type I (nas, brg, lam, stpl, stpr) or the Type II (prosH, ssp, prosM, ops, bas, jugr, zygoor, dacr, dacl, zygool, jugl, mastr, mastl) point over any model type. The use of the Coefficient of Determination (COD) reflects the estimation of predictability of the direct digital landmark points by the selection of landmarks using the process models. The COD values indicate that there is variation in the estimation of the predictive quality of

landmark points selected from process models for the direct digital landmark points.

Chapter Five

Discussion

The results of these tests of processing parameters and correlation are positive in indicating the overall correspondence by correlation of the landmark points selected from the process parameter models with that of the criterion direct digitizer landmark point selections.

Model processing

The processing procedures applied to the raw mesh models all accomplished the goal of reducing the computational parameters of the models. This reduction had the effect of not only improving the access and utility of the models for research and analysis in a typical computer environment, but also of equalizing the models for face and vertex counts for all models within each set of process parameters.

Subjective observer experience working with the models from each of the four processes found the visual representation of the original raw models to be best represented by the high-face count models. However, the non-manifold processes were more of a challenge to make use of for the landmark selection procedure.

Validity

The validity of the model under study in this research is based on the theory that positive correlation can be determined between the criterion measurement and the measurements under examination if they are both measuring the same thing. This concept is applied to the sample of the Yacchi-no-gamma crania that have been subjected to 3-D data collection using 3-D surface scans and Microscribe®

(Revware, Raleigh, NC, USA) landmark point digitizing. Landmarks derived from digital models having undergone each one of two levels of processing parameters to result in four models were analyzed for correlation to the set of landmarks collected using the direct digitizing method using two analytical schemes.

There is an expectation based on these definitions that Type I landmarks with have the most conservative variability between samples of the same point. Type II landmarks are slightly less conservative, and Type III landmarks are expected to show the most variation between point samples. If the correlations of the sampled landmark points and the Microscribe® (Revware, Raleigh, NC, USA) digitizer landmark points indicate any separation within the definitions of Type I, II, and III landmarks; such a pattern should not be classified as a type of random error because it is caused by documented effect of the definition of the landmark point.

Paired Inter-Landmark Distance

The use of Paired Inter-Landmark Distance (ILD) is applied here as a linear translation of the three dimensional data. This puts this research in line with both previous craniometric studies in both two and three dimensions.

Fatah et al. (2014) determined that the differences between the mean of direct measurements and model measurements for the sample in their study were within a distance of 2mm. The authors defined this as within the acceptable range of variation for error of craniometric measurements.

For ILD, the average distance between the direct digitizer inter-landmark distances and the process inter-landmark distance was less than 2 mm over all

landmarks over all processes for all Types. This is within the margin determined by Fatah et al. (2014).

For the results of this analysis, validity is determined by the calculation of several correlation coefficients. With the agreement of the data for the two types of analysis with the findings of previous research, so long as our correlation is good and positive, we can consider it sufficient to validate the data collected for the process models. As we find our overall correlation of the Inter-Landmark Distances to be $\sim r$=83 or better for all processes, it is reasonable to conclude for validity of the landmark points derived from all process models and consider all combinations of the processing parameters to be representative of the original physical materials they represent.

There are landmarks with characteristics that result in a higher variability even when selected by the same observer in the same or different sessions. These landmarks have a very loosely bound definition and often are difficult to locate by definition using the Microscribe® (Revware, Raleigh, NC, USA) (Ross and Williams 2008; Sholts et al. 2011a). ANOVA GLM was applied with R software (Team 2014) and suggests the relative distance differences from the paired ILD of the highlighted eight out of the 37 total sampled landmarks as having a higher relative variability.

Applying a General Linear Model of an Analysis of Variance test to the ILD samples values allows for the consideration of whether the values are likely given the criterion values of the direct digital sample, or if they could have occurred randomly. The resulting high values of the F-Statistic and very low values of the p-

value, it is reasonable to conclude that the values of the ILD sample are not due to chance.

Of those landmarks indicating a higher variability under ANOVA GLM, none were among the eight landmarks with missing values. Landmarks with missing values are listed in Table 6, and generally indicated high correlation. Removal and re-analysis of the correlation of ILD did not indicate a strong influence on correlation caused by the imputation of missing values.

These eight landmarks are defined by Bookstein (1997) as Type II or Type III, and represent all the landmarks for any process correlation coefficient less than .8 for the ILD analysis. This refutes a conclusion of random error for the measurement of these landmarks due to the noted definitional variation acting on the point samples of these landmarks.

Landmark Point Variation

The use of Landmark Point Variation is applied here to evaluate the spatial relationship of individual point selection given the multiple processing methods. This portion of the analysis relies on the three dimensional relationship between the selected locations of each point for each processing method.

Although this is divergent from the types of craniometric study typically applied to craniometric studies within anthropology, such lines of inquiry are to be found in medical and surgical research. This is especially significant to the forensic aspects of biological anthropology and considers the importance of high dimension imaging technology applied to medical and surgical studies.

Olszewsk, et al. (2010) investigate the accuracy and reproducibility of landmarks given various methods of collection. These authors are investigating landmark collection in terms of the scatter introduced by repeated landmark selection by observers and using selection models that differed. This article forms the basis for the Landmark Point Variation study applied for this research.

When examining the preliminary plot of distance data for correlation, the values for the Microscribe® (Revware, Raleigh, NC, USA) distance are higher than the values of the distances between processes for each process coordinate point for all but one landmark. This indicates that the distance between a process point and all other process points is less than the distance between the process point and the digitizer point for that landmark.

The results of the Mantel's test of Correlation were strong enough to find in favor of validity by correlation for most landmarks of the LPV sample. It was notable, however, that for this analysis of the scatter of selected landmarks, the manifold processes had a higher correlation value than for the non-manifold processes. This would suggest that the processes that applied manifold adjustments did result in some calculable improvement to the surfaces of the models and resulted in landmark point selection that was slightly more correlated to the landmark point selection of the direct digitizer landmarks.

Given that the collection of landmark points for all process models was randomized, and the selected points on the models could be reviewed in the digital selection software, learning is not likely to be a viable conclusion for the differences in correlation between the non-manifold and manifold process models. With this consideration, it is reasonable to conclude that the landmark point selection from

neither the manifold processes or the non-manifold models result in significant systematic bias or error.

Porion (porr, porl) is used as an alignment landmark, therefore variation between the process models and the digitizer landmarks might be artificially reduced. The plots of the values for the distances between processes for the porion landmark points (left and right) indicate very low variation. In the measurement scale applied here; the differences are less than one millimeter. The scatter of the sample observations of porion are actually distributed on a fairly wide field, especially when considered against the scatter distribution of the other points.

Supraglabellare (spglb) landmark points have significantly different coordinate locations between the process samples collected from the 3-D models from the Microscribe® (Revware, Raleigh, NC, USA) Digitizer observation. This is due to both the significantly different definitions applied by the observers and the difference in the observation of the landmark in cross-section. Supraglabellare is a significant in defining anterior projection of the frontal and nasal bones along the midline (Howells 1973). Variations are inherent to measures based off supraglabellare due to difficulties selecting directly by lateral observation, or on a lateral cephalograph (x-ray). Strictly defined as a midline structure, the point should be most accurately collected from a properly aligned cranium in cross-section. If the crania is not perfectly aligned, or the observer is collecting point from a 2D image, the points will be much less likely to closely match between different observations, observers, or selection methods.

Prosthion *(Howells)* (prosH), subspinale (ssp), and prosthion *(Martin)* (prosM), are mid-line and all Type II (Ousley 2010). Located on fragile maxillary

Howells (1973) discusses the deferential definitions that have been historically applied to prosthion. The prosthion selections for both the Howells and Martin definition are included in the ThreeSkull software (Ousley 2010) apply slightly different definitions of the location of prosthion.), Points 4-11 are mid-line and can reflect differences in overall size. Three are Type III; glabella (glb), supraglabellare (spglb), and opisthicranion (ops)] - having measurements that are dependent upon the orientation of the crania during sample. Three are Type I; nasion (nas), bregma (brg), lambda (lam) and are dependent upon the visual evaluation of the intersection of cranial sutures (Bookstein 1997; Ousley and McKeown 2001).

Right and Left paired lateral craniofacial landmark points are both collected and with the exception of the orbital height landmarks (obhi, obhs) for all crania. When the lateral landmarks are considered separately, the left craniofacial landmarks are slightly more correlated to the digitizer landmarks than the right or all processes, which agrees with the findings of several previous studies (McKeown and Jantz 2005; Jantz et al. 2013).

Interpretations

Based on the statistical analysis of validity applied to this sample, the hypothesis of convergence of Landmark Point Variation and Inter-Landmark Distance are retained. Insufficient evidence is found to reject convergence and conclude in favor of the null hypothesis, which would have required significant differences between the selected landmark points and inter-landmark distances for one or more processes.

The differences between processed models and the resulting variations accumulated from the selection of landmarks from processed models are consistent

with the expectations of the Bookstein Landmark Types for all methods of processing.

The evaluation of the Coefficient of Determination for the ILD sample suggests strongly that the use of all methods processing result in landmarks collected from digital models that are robust against landmark methods proposed by previous research in the medical and biological anthropology fields.

The evaluation of the LVP sample Coefficient of Determination suggests that the use of manifold methods of processing results in landmarks collected from digital models that are in agreement with previous research in the medical and biological anthropology fields.

The selection of a process parameter for future data collection, transmission, and research – based on the results and conclusions determined by this research indicate all of the process parameters are acceptable in reduction of file size and retention of data for the purposes of landmark point selection. When further considered in terms of the post-hoc, the LPV analysis indicates that manifold models present the best replication of landmark selection overall.

Limitations and Possible Sources of Error

This thesis has an experimental design for validity testing without reliability testing and without replication. The omission of those factors does not suggest they have been ignored or there was a failure to consider them. The notions of observer bias and error are significant. This thesis is less concerned with testing for these types of error for the fact that there is not test of a population or biological factor under examination. The tests here have examined the extensibility of the single

source sample analysis of Jantz et al. (2013), Williams and Slice (2010), Garvin and Ruff (2012), Sasо et al. (Saso et al. 2011), Fukumine et al. (2006) and others to an archaeological sample and collaborative data collection.

A pair of potential sources of error which present for consideration are the temporal and preservation aspects of the physical data collection. At the time of collection of the Microscribe® digitized landmark points, the crania were reported to be in a marked state of physical decline, which the researchers – Beatrix Dudzik (2012), and Noriko Seguchi (2010) – attributed to the storage conditions of the collection. At the time the digitizer landmark points were collected, Dudzik was obliged to use a thin sheet of vinyl to protect the surface of the crania from contact with the Microscribe® (Revware, Raleigh, NC, USA) probe. This should have at most a nominal effect on the location of landmark points, but it should be considered for introducing the possibility of error. The two year time span between the collection of the two cranial samples may have also introduced a degree of error. If the collection is deteriorating in the present storage conditions, it is probable that deterioration would cause variable inconsistencies between the samples. When these possible sources of error are considered together, they become less likely to present a significant and directional source of error. First, the application of the vinyl between the crania and the probe would have most likely resulted in a slight dimensional increase in measurements derived from the digitized data. This would be in contrast the loss of material that would most likely accompany deterioration of the materials.

Chapter Six

Conclusion

Findings of validity of the use of landmark points selected from 3-D mesh models derived using the process parameters applied in this thesis find in favor of the hypothesis of convergence. Findings are further in line with the expected variations that result from the definitions (Type I, II and III) of the landmarks points and the impact less constrained definitions have on the values of the correlation tests. Positive values of the tests of correlation indicate the validity of landmark points selected from all processes against the landmark points selected for the criterion direct digitizer point selection. The Paired Inter-Landmark Distance average distance between process landmark points and criterion direct digitizer landmark points is less than the margin suggested by previous research. Overall correlation is good and positive and ANOVA GLM results are in favor of a conclusion that the results found were unlikely to be due to chance. Reproducibility, represented by Landmark Point variation of landmark point selection for each process method against the criterion direct digitizer method landmark point selection is favorable for all processes indicated by the Mantel Tests of correlation. Also indicated was a stronger correlation of the manifold process parameter landmark points over the non-manifold process landmark points. This significantly suggests that an aspect of the manifold process parameter improves the reproducibility of landmark point selection on process models against the criterion direct digitizer landmark point selection on the physical materials.

This thesis is based in a methodological research framework. As such, it looks to validate solutions to the difficulties of performing research on materials

that are limited and fragile by nature. Selecting from one of the many data acquisition methods available in 3-D (CT, Surface scan, Photogrammetry, Point digitizing), the sheer amount of data that can be captured is staggering. However, a massive quantity of data must be rendered functional for the purposes of meaningful interpretation. With 3-D data specifically, it must be held to a level that is true to the original materials, but still functional for study in a digital environment. This means processing of raw data.

A further consideration for the design of this study was the nature of the acquisition and dissemination of the collected data. The data was collected using two different methods, at different times each by a single researcher. This kind of disparate data collection enables researchers to overcome difficulties of time and distance, opening avenues of research that would otherwise be closed. It is difficult to undertake studies of human remains in the simplest of circumstances. When negotiations with foreign governments, limited access, and preservation become roadblocks, little recourse is available to the researcher. To be able to study virtual materials is one solution to the problems described above.

There are problems remaining to be overcome for the purposes of future methodological development and applied research using 3-D models. Sutures represent significant features which can still be difficult to examine from 3-D models (Saitou et al. 2011). Scans are taken using medical imaging technology and monochromatic surface scans lack reference from the surface texture (digital imaging definition of texture, which would refer to the color variation of the real object). Dry skulls scanned with color sensitive equipment generally overcome this issue to a similar degree that the same features can be visually detected. The issue

of texture highlights the variation in samples that results from the use the different methods of craniometric data collection. However, testing new methods against the benchmark methods grants researchers the ability to move forward without sacrificing the work that has come before.

Appendices

Appendix 1: Landmark Definitions and References

The definitions of classifications of landmarks are derived from Bookstein (1991) and describe the characteristics of each type:

Type I landmark : Landmark defined at a structural location with strong homology. Sutural intersections are the most typical landmarks of this type related to craniometric measurements.

Type II landmark: A geometric or non-dependent extremal point defined by a structure. This could mean an apex of a curve or the end of a bony process.

Type III landmark: A landmark with a location dependent upon orientation, distance, or structural development. Height and breadth measurements would fall under this category. This category would be expected to have the greatest variability between observations of the same subject, and between subjects due to the dependency factor and broad definitions.

Appendix 2: Cranial Sample

The Cranial Sample Consists of Materials Excavated from the Yacchi-no-gamma (Yacchi Cave), Kumejima (Kume Island) in the Okinawa Prefecture and housed at the Okinawa Prefectural Archaeology Center, Okinawa Japan. The sex of the crania in the sample is presumed to be correct as noted within the collection. The demographic information for this sample does not include age estimation.

8-14_f

3. 8-14_f

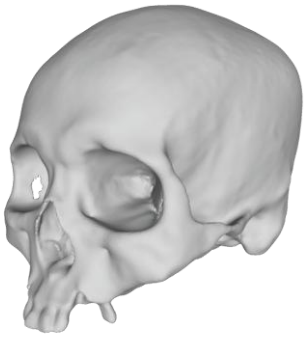

11-5_m

4. 11-5_m

11-14_f

5. 11-14_f

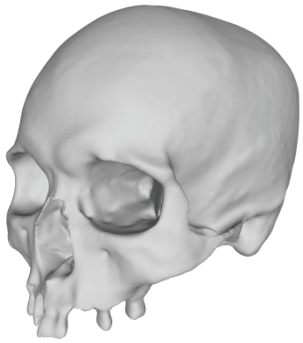

11-15_m

6. 11-15_m

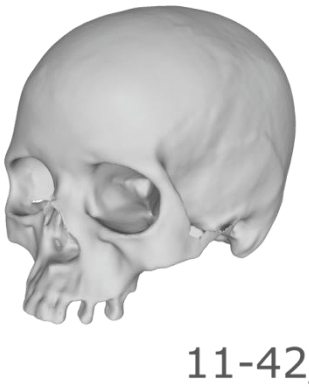

7. 11-42_f

8. 2go-2-30_m

9. 2go-2-32_m

10. 7-12_m

11. 9-15_f

12. 11-34_m

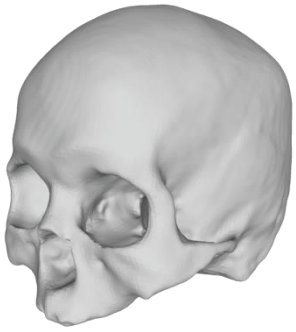

11-42_m

13. 11-42_m

Appendix 3: Model Processing Protocol

1. Merge superior and inferior hemispheres of cranial raw models and refine alignment to the overall d^2 for overlapping regions. Flatten dual model mesh into a single model mesh file.
2. Align to single mesh model to Frankfurt Horizontal Plane.
3. Manifold Version High Face count
4. Manifold Version Low Face count
5. Non-Manifold Version High Face count
6. Non-Manifold Version Low Face count

   Figure 1: Examples of Processed Models
7. Save all versions to the appropriate naming convention and record the final file size for all versions.

   Table 5: Computational Characteristics of Processed Models

Appendix 4: Data Collection Protocol

1. Import processed meshes into Stratovan Checkpoint
2. Collect landmark points in order as indexed

   Table 1: Landmarks for 3-D Comparison.

   Figure 4: Landmark Map

   Figure 5: Example of Landmark Point Sample
3. Export landmark point coordinates as comma separated value (*.CSV) files.

Appendix 5: Direct Digitizer Landmark Point Processing

Direct digitizer landmarks were collected by Beatrix Dudzik (2012) with the Microscribe® (Revware, Raleigh, NC, USA) G2 3-D Digitizer. Data was collected directly from crania of the Yacchi-no-gamma sample and indexed with 3Skull Software (Ousley 2010). Data was exported from the indexing software to Microsoft Excel © spreadsheet file format.

The landmark point data for each crania went through the following processing steps to prepare for the Landmark Point Variation and ILD comparison analyses.

1. Align the set of landmark points for each crania to the Frankfurt Horizontal Plane using Bookstein Alignment method and correction (Slice 2013).

Figure 6: Stages of Bookstein Alignment

Equation 1: Bookstein Superimposition Transformation - Unit - Scale (Lele 2001)

Equation 2: Bookstein Superimposition Transformation - Plane - Rotation (Lele and Richtsmeier 2001)

Equation 3: Bookstein Superimposition Transformation - Root – Translation (Lele and Richtsmeier 2001)

Equation 4: Bookstein Superimposition Transformation – Correction for Standard Coordinate System

Appendix 6: Statistical Analysis Methods

Pearson's product-moment correlation coefficient (Press 1992)

To compute the sample correlation *r*: $r_{yx} = \frac{\sum_i (x_i - \bar{x})(y_i - \bar{y})}{\sqrt{\sum_i (x_i - \bar{x})^2 \sqrt{(y_i - \bar{y})^2}}} = \frac{S_{xy}}{\sqrt{S_{xx} S_{yy}}}$

And test the two-tailed significance *t*:

$$t = r \sqrt{\frac{n-2}{1-r^2}}$$

Spearman's rank order correlation coefficient (Press 1992)

To compute the non-parametric equivalent to the Pearson's *r*; converting the *x* and *y* values to a ranks (assuming no ties) r_s:

$$r_s = \frac{\sum_i (R_i - \bar{R})(S_i - \bar{S})}{\sqrt{\sum_i (R_i - \bar{R})^2} \sqrt{\sum_i (S_i - \bar{S})^2}}$$

and calculating significance as before:

$$t = r_s \sqrt{\frac{n-2}{1-{r_s}^2}}$$

Analysis of Variance (GLM)

R Sample Formula

```
        ctl     <-      c ( prosH$dd )

        trt     <-      c ( prosH$hf )

group  <-       gl( 2, 468, 936, labels = c( "Criteria" , "High Face") )

weight <-       c ( ctl, trt)

lm.prosH        <-      lm ( weight ~ group )

lm.prosH0       <-      lm ( weight ~ group - 1 )


anova(lm.prosH)

summary(lm.prosH0)


out.anova.lm.prosH          <-  capture.output(  anova( lm.prosH) )

cat(out.anova.lm.prosH      ,file="1-Analysis/CID ANOVA.txt",sep="\n",append=TRUE)


out.summary.lm.prosH0   <-  capture.output(  summary( lm.prosH0) )

cat(out.summary.lm.prosH0   ,file="1-Analysis/CID ANOVA.txt",sep="\n",append=TRUE)
```

An ANOVA Extension of the t-test using a correlation coefficient to describe the relationship of quantitative data.

GLM is equivalent to a multiple regression analysis but suited to multiple variables. Use to "predict" variation of the dependent variable given the observed values of the independent

Significance is tested as an F statistic with a p-value. The F statistic is compared to the critical value of F and the p-value is compared to the alpha level. The F statistic explains if the model (prediction) explains the observed values. The p-value indicates whether the strength of the prediction is statistically significant.

Mantel Test of Correlation (Hammer et al. 2001; Sokal and Rohlf 2011)

The correlations of two matrices are evaluated by the Pearson's correlation coefficient (Equation 7) of the matrix elements.

Process Model Euclidean Distances

$$\begin{bmatrix} 0 & & & & & \\ a & 0 & & & & \\ f & b & 0 & & & \\ j & g & c & 0 & & \\ m & k & h & d & 0 & \\ o & n & l & i & e & 0 \end{bmatrix}$$

Criterion Direct Digital Euclidean Distances

$$\begin{bmatrix} 0 & & & & & \\ A & 0 & & & & \\ F & B & 0 & & & \\ J & G & C & 0 & & \\ M & K & H & D & 0 & \\ O & N & L & I & E & 0 \end{bmatrix}$$

$$r_{yx} = \frac{\sum_i (x_i - \bar{x})(y_i - \bar{y})}{\sqrt{\sum_i (x_i - \bar{x})^2 \sqrt{(y_i - \bar{y})^2}}} = \frac{S_{xy}}{\sqrt{S_{xx} S_{yy}}}$$

This application of the Mantel's test of correlation used the Euclidean Distance values of each data elements from the origin to populate the matrices.

$$t = 2(r \sqrt{\frac{n-2}{1-r^2}})$$

Test of significance involves random permutation of the matrix elements an re-evaluation of the Pearson's correlation coefficient *r*. Multiple replications of random permutations of the matrices (9999 permutations applied by default in PAST 3) give a series of computed *r* values to compare to the original calculation of the matrix correlation to determine the probability of the original correlation coefficient. The resulting p-value is a one-tailed.

Appendix 6: Definition of Terms (Glossary)

Terms used in specific context for 3-D rendering, multi-dimensional processing, and biological metrology.

Allometry: Term used to describe the variations in shape that follow changes in size in biological forms.

Asterion: Intersection of the sutures between the posterior temporal, inferior parietal and lateral occipital bones (White and Folkens 2000)

Atlas: A model based the averages of the dimensions of the model sample units.

Bookstein (Shape) Alignment: Superimposition method that sets a primary coordinate as the forced origin and a secondary coordinate.

Calibration Surface: A surface placed inside a scanning environment having one or more calibration marks used by the scanner optical processing to aid alignment and orientation calibration of the surfaces to be captured. Can be considered compared to photographic scales.

Decimation: A process applied to a 3-D mesh to re-distribute vertices and faces. Depending on the desired outcome, the parameters can be uniform distribution, clustered distribution, and targeted control of the final number of vertices and faces.

Discretization: the process of dividing geometry into finite elements to prepare for analysis.

Euclidean Distance: The separation between two points in a 2 or 3-dimensional space represented by a vector the length of the square root of the sum of the squared differences of the values of *x, y,* (and *z)* of the two points.

Face(s): flat polygons of a 3-D mesh defined by the intersection of vectors between vertices of the mesh.

Frankfurt Horizontal: Orientation of the cranium attributed to Paul Broca in the 19^{th} century. Define as a plane transecting the left and right porion landmarks and the landmark defining the left lateral intersection of the orbital rim and the zygoorbital suture - for my purposes, zygoorbitale left. (White and Folkens 2000)

Generalized Procrustes Alignment (GPA): Superimposition method that projects non-affine (no shear) transformation of shapes into the alignment which minimizes the distance squared (d^2) between homologous points.

Homology: The similarity of structures that is due to relatedness, in this case the translation of genetic template shared by related individuals into the developed structures of the cranium.

Landmark: In the text; *landmark* refers to a definition of a location, *point* refers to a sample coordinate of a landmark.

Landmark Point Variability: Sample Subset composed of the distances between 1) The process model and digitizer point coordinates of an individual landmark (four models and one digitizer observation), for 2) Each process (four processes), for 3) Each crania (n=13), and for 4) Each landmark (n=37).

Manifold: In digital modeling terminology, manifold refers to rendering a model as solid and geometrically possible. This is necessary due to the need for an object to have consistent and defines sides or thickness to exist. As an example, in a 3-D model, it is possible for adjacent faces to be defines as being internal and external. That is not possible in a physical object. If you punched a hole through a piece of paper, the edges of the hole have a physical dimension between the flat sides of the paper.

Mesh Model: A three dimensional model composed of inter-connected point-cloud vertices and surfaces defined between the interconnections of the vertices (faces).

Meta-data: Information about a digital file that includes file dimensions and relevant parameters to the type of data in the file. 3-D mesh meta-data would include the total number of faces and vertices.

Normalized Vector: A construct of 3-D digital geometry that orients perpendicular to a face or point in 3-D space and is used to base the definition of outer and inner directions of a face.

Paired Inter-Landmark Distances: Sample subset composed of Euclidean distances derived from the distance between 1) A primary landmark and all other unique landmarks sampled (36 distances for each of 37 landmarks), for 2) Each process model (four), and for 3) Each crania (n=13).

Registration: The alignment of a 3-D object (e.g., mesh, or point cloud, or point sample) to either a specific coordinate system, to another 3-D object, or other specific configuration.

Texture: Defined in terms of 3-D modeling and rendering, refers to color images projected over the 3-D mesh rendered either per vertex or face (Cignoni, 2014)

Transformation matrix: An *n+1*dimensional matrix that records the mathematical translational, rotational, or scale change in the location of a point when it has been moved or superimposed.

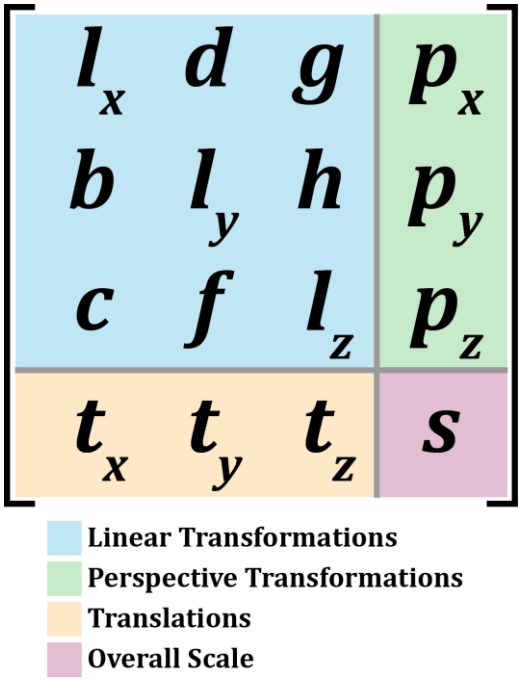

Figure 11: Transformation Matrix Structure (Rogers and Adams 1990; Mortenson 2007)
Transformation matrix is represented in homogeneous coordinates which due to their nature of representing an infinite projection of a point from the origin can be more easily be applied to a coordinate than the Euclidean counterpart. This type of matrix can be used to represent all the necessary changes to the location of a point when transformation is applied. The changes to the location include translation, rotation, scale, and shear.

Vertex (vertices):Points of a 3-D mesh that represent the geometry of the mesh in multi-dimensional space.

Zygotemporale: The superior or inferior most point on the suture between the zygomatic and temporal bone on the zygomatic process.

References cited

Z Corporation Introduces ZScanner 800 Handheld 3D Scanner with 5x Increase in Resolution. In: Z-Corp(3Dsystems), editor.

Abdel Fatah EE, Shirley NR, Jantz RL, and Mahfouz MR. 2014. Improving Sex Estimation from Crania Using a Novel Three- dimensional Quantitative Method.(Report). Journal of Forensic Sciences 59(3):10.

Athreya S. 2006. Patterning of geographic variation in Middle Pleistocene Homo frontal bone morphology. Journal of Human Evolution 50(6):627-643.

Bass WM. 2005. Human osteology : a laboratory and field manual. Springfield, Mo.: Missouri Archaelogical Society.

Bookstein FL. 1997. Morphometric tools for landmark data: geometry and biology. Cambridge [England]. New York: Cambridge University Press.

Carmines EG, and Zeller RA. 1979. Reliability and validity assessment. Beverly Hills, Calif.: Beverly Hills, Calif. : Sage Publications.

Cignoni P, Callieri M, Corsini M, Dellepiane M, Ganovelli F, and Ranzuglia G. 2008. MeshLab: an Open-Source Mesh Processing Tool.

Cignoni P, and Scopigno R. 2008. Sampled 3D models for CH applications: A viable and enabling new medium or just a technological exercise? J Comput Cult Herit 1(1):1-23.

Consortium JAHPG, T J, N N, M H, S K, H O, K U, R K, J O, A T et al. . 2012. The history of human populations in the Japanese Archipelago inferred from genome- wide SNP data with a special reference to the Ainu and the Ryukyuan populations. Journal of Human Genetics 57(12):787.

Dudzik B. 2012. 3D Coordinate landmarks from a cranial sample of the Yacchi-no-gamma osteological materials, Kumejima, Okinawa, Japan. In: Dudzik B, editor. Unpublished.

Ercan I, Guney I, Ocakoglu G, and Yazici B. 2008. Adaptation of generalizability theory for inter-rater reliability for landmark localization.

Fukase H, Wakebe T, Tsurumoto T, Saiki K, Fujita M, and Ishida H. 2012. Facial characteristics of the prehistoric and early-modern inhabitants of the Okinawa islands in comparison to the contemporary people of Honshu. Anthropological Science 120(1):23-32.

Fukumine T, Hanihara T, Nishime A, and Isida H. 2006. Nonmetric cranial variation of early modern human skeletal remains from Kumejima, Okinawa and the peopling of the Ryukyu Islands. Anthropological Science 114:141-151.

Garvin HM, and Ruff CB. 2012. Sexual dimorphism in skeletal browridge and chin morphologies determined using a new quantitative method. American Journal of Physical Anthropology 147(4):661-670.

Girardeau-Montaut D. 2014. Cloud compare - Open Source Project. http://www.cloudcompare.org: *CloudCompare - Open Source Project*.

Graw M, Czarnetzki A, and Haffner H-T. 1999. The form of the supraorbital margin as a criterion in identification of sex from the skull: investigations based on modern human skulls. American Journal of Physical Anthropology 108(1):91.

Hale AR, Honeycutt KK, and Ross AH. 2014. A Geometric Morphometric Validation Study of Computed Tomography–Extracted Craniofacial Landmarks. Journal of Craniofacial Surgery 25(1):231-237.

Hammer Ø, Harper DAT, and Ryan PD. 2001. Paleontological statistics software package for education and data analysis. Palaeontological Electronica 4(1):9.
Hoppe H. 1999. New quadric metric for simplifiying meshes with appearance attributes. Proceedings of the conference on Visualization '99: celebrating ten years. San Francisco, California, USA: IEEE Computer Society Press. p 59-66.
Hoppe H, DeRose T, Duchamp T, McDonald J, and Stuetzle W. 1993. Mesh optimization. Proceedings of the 20th annual conference on Computer graphics and interactive techniques. Anaheim, CA: ACM. p 19-26.
Howells WW. 1973. Cranial variation in man; a study by multivariate analysis of patterns of difference among recent human populations. Cambridge, Mass.: Cambridge, Mass., Peabody Museum of Archaeology and Ethnology, Harvard University.
Howells WW. 1996. Howells' Craniometric Data on the Internet. AMERICAN JOURNAL OF PHYSICAL ANTHROPOLOGY 101:441-442.
Hsaio TH, Chang HP, and Liu KM. 1996. Sex determination by discriminant function analysis of lateral radiographic cephalometry. Journal of Forensic Science Volume 41(Issue 5):792-795.
Hsiao T-H, Tsai S-M, Chou S-T, Pan J-Y, Tseng Y-C, Chang H-P, and Chen H-S. 2010. Sex determination using discriminant function analysis in children and adolescents: a lateral cephalometric study. Int J Legal Med 124(2):155-160.
Huber PJ. 1981. Robust statistics. New York: New York : Wiley.
Jantz R, Mahfouz M, Shirley NR, and Abdel Fatah E. 2013. Improving Sex Estimation From Crania Using 3-dimensional CT Scans. https://www.ncjrs.gov/pdffiles1/nij/grants/240688.pdf: U.S. Department of Justice.
Kazhdan M, Bolitho M, and Hoppe H. 2006. Poisson Surface Reconstruction.
Kim M, Huh K-H, Yi W-J, Heo M-S, Lee S-S, and Choi S-C. 2012. Evaluation of accuracy of 3D reconstruction images using multi-detector CT and cone-beam CT. Imaging Sci Dent 42(1):8.
Klingenberg CP. 2010. Evolution and development of shape: integrating quantitative approaches. Nature Reviews Genetics 11:623-635.
Koganebuchi KAE, Katsumura T, Nakagome S, Ishida H, Kawamura S, Oota H, and The Asian Archival Dna Repository C. 2012. Autosomal and Y-chromosomal STR markers reveal a close relationship between Hokkaido Ainu and Ryukyu islanders. Anthoropol Sci 12(3): 199-208
Lele S. 2001. An invariant approach to statistical analysis of shapes. Boca Raton, Fla.: Boca Raton, Fla. : Chapman & Hall/CRC.
Lele S, and Richtsmeier JT. 2001. An invariant approach to statistical analysis of shapes. Boca Raton, Fla.: Boca Raton, Fla. : Chapman & Hall/CRC.
Mahfouz MR, Merkl BC, Abdel Fatah EE, Booth R, and Argenson JN. 2007. Automatic methods for characterization of sexual dimorphism of adult femora: distal femur. Computer Methods in Biomechanics and Biomedical Engineering 10(6):447-456.
McKeown A, and Jantz R. Comparison of Coordinate and Craniometric Data for Biological Distance Studies.215-230.
Moiseyev VG. 2009. ON THE ORIGIN OF THE RYUKYU ISLANDERS: THE INTEGRATION OF CRANIOMETRIC AND CRANIAL NONMETRIC DATA. Archaeology, Ethnology and Anthropology of Eurasia 37(4):146-152.

Mortenson ME. 2007. Geometric transformations for 3D modeling. New York: Industrial Press.
Muramatsu A, Nawa H, Kimura M, Yoshida K, Maeda M, Katsumata A, Ariji E, and Goto S. 2008. Reproducibility of maxillofacial anatomic landmarks on 3-dimensional computed tomographic images determined with the 95% confidence ellipse method. Angle Orthod 78(3):396-402.
Nance JD, and Ball BF. 1986. No Surprises? The Reliability and Validity of Test Pit Sampling. American Antiquity 51(3):457-483.
Olszewski R, Cosnard G, Macq B, Mahy P, and Reychler H. 2006. 3D CT-based cephalometric analysis: 3D cephalometric theoretical concept and software. Neuroradiology 48(11):853-862.
Olszewski R, Frison L, Wisniewski M, Denis JM, Vynckier S, Cosnard G, Zech F, and Reychler H. 2013. Reproducibility of three-dimensional cephalometric landmarks in cone-beam and low-dose computed tomography. Clin Oral Investig 17(1):285-292.
Olszewski R, Reychler H, Cosnard G, Denis JM, Vynckier S, and Zech F. 2008. Accuracy of three-dimensional (3D) craniofacial cephalometric landmarks on a low-dose 3D computed tomograph. Dentomaxillofac Radiol. England. p 261-267.
Olszewski R, Tanesy O, Cosnard G, Zech F, and Reychler H. 2010. Reproducibility of osseous landmarks used for computed tomography based three-dimensional cephalometric analyses. J Craniomaxillofac Surg. Scotland. p 214-221.
Olszewski R, Zech F, Cosnard G, Nicolas V, Macq B, and Reychler H. 2007. Three-dimensional computed tomography cephalometric craniofacial analysis: experimental validation in vitro. Int J Oral Maxillofac Surg. Denmark. p 828-833.
Ousley S, and McKeown A. 2001. Human Remains: Conservation, Retrieval and Analysis : Proceedings of a Conference Held in Williamsburg, VA, Nov. 7-11th 1999. In: Williams E, editor. BAR international series: Archaeopress. p 173-184.
Ousley SD. 2010. Threeskull. Version 2.0.
Pinto SD, Cesar Jr. R, and Urbanová P. 2013. Analysis of Supraorbital Margins in human skull for characterization of sexual dimorphism. In: Cuadros-Vargas A, and Cayllahua Cahuina EJY, editors. SIBGRAPI (The Conference on Graphics, Patterns, and Images) 2013. Arequipa Peru: SIBGRAPI (The Conference on Graphics, Patterns, and Images) 2013. p 1-4.
Rogers DF, and Adams JA. 1990. Mathematical elements for computer graphics. New York: McGraw-Hill.
Ross AH, Slice DE, and Williams SE. 2010. Geometric Morphometric Tools for the Classification of Human Skulls. https://www.ncjrs.gov/pdffiles1/nij/grants/231195.pdf: U.S. Department of Justice.
Ross AH, and Williams S. 2008. Testing Repeatability and Error of Coordinate Landmark Data Acquired from Crania*. Journal of Forensic Sciences 53(4):782-785.
Saitou N, Kimura R, Fukase H, Yogi A, Murayama S, and Ishida H. 2011. Advanced CT images reveal nonmetric cranial variations in living humans. Anthropological Science 119(3):231-237.

Saso A, Matsukawa S, and Suwa G. 2011. Comparative analysis of the glabellar region morphology of the late Pleistocene Minatogawa crania: a three-dimensional approach. Anthropol Sci 119(2):113-121.
Seguchi N. 2010. 3D surface scans of a sample of crania from the Yacchi-no-gamma, Kumejima, Okinawa, Japan osteological collection. In: Seguchi N, editor. Unpublished.
Shearer BM, Sholts SB, Garvin HM, and Wärmländer SKTS. 2012. Sexual dimorphism in human browridge volume measured from 3D models of dry crania: A new digital morphometrics approach. Forensic Science International 222(1-3):400.e401-400.e405.
Sholts SB, Flores L, Walker P, and Warmlander S. 2011a. Comparison of Coordinate Measurement Precision of Different Landmark Types on Human Crania Using a 3D Laser Scanner and a 3D Digitiser: Implications for Applications of Digital Morphometrics. Int J Osteoarchaeol 21(5):535-543.
Sholts SB, Walker PL, Kuzminsky SC, Miller KWP, and Wärmländer SKTS. 2011b. Identification of group affinity from cross- sectional contours of the human midfacial skeleton using digital morphometrics and 3D laser scanning technology. Journal of forensic sciences 56(2):333.
Sholts SB, Wärmländer SKTS, Flores LM, Miller KWP, and Walker PL. 2010. Variation in the Measurement of Cranial Volume and Surface Area Using 3D Laser Scanning Technology. Journal of Forensic Sciences 55(4):871-876.
Slice D, McKeown A, and Jantz R. 2005. Comparison of Coordinate and Craniometric Data for Biological Distance Studies. Modern Morphometrics in Physical Anthropology: Springer US. p 215-230.
Slice DE. 2013. Morpheus et al., Java Edition. Department of Scientific Computing.
Smith NE, and Strait SG. 2008. PaleoView3D: from specimen to online digital model. Palaeontologia Electronica 11(2):1.00.
Sokal RR, and Rohlf FJ. 2011. Biometry. W. H. Freeman.
Team RC. 2014. R: A language and environment for statistical computing. R Foundation for Statistical Computing. In: Team RC, editor. Vienna, Austria.
Thayer ZM, and Dobson SD. 2010. Sexual dimorphism in chin shape: Implications for adaptive hypotheses. American Journal of Physical Anthropology 143(3):417-425.
Walker PL. 2008. Sexing skulls using discriminant function analysis of visually assessed traits. American Journal of Physical Anthropology 136(1):39-50.
Weinberg SM, and Kolar J. 2005. Three-dimensional surface imaging: Limitations and considerations from the anthropometric perspective. Journal Of Craniofacial Surgery 16(5):847-851.
White TD, and Folkens PA. 2000. Human osteology. San Diego: San Diego : Academic Press.
Williams SE, and Slice DE. 2010. Regional shape change in adult facial bone curvature with age. American Journal of Physical Anthropology 143(3):437-447.
Wong JY, Oh AK, Ohta E, Hunt AT, Rogers GF, Mulliken JB, and Deutsch CK. 2008. Validity and Reliability of Craniofacial Anthropometric Measurement of 3D Digital Photogrammetric Images. The Cleft Palate-Craniofacial Journal 45(3):232-239.

Zaiontz C. Real Statistics Using Excel. In: Zaiontz C, editor. p Real Statistics Website.